https://doi.org/10.5194/tc-2020-217
Preprint. Discussion started: 7 September 2020


The Cryosphere Discussions
Open Access
EGU

# Pervasive diffusion of climate signals recorded in ice-vein ionic impurities

Felix S. L. Ng[1]

[1]Department of Geography, University of Sheffield, Sheffield, UK

*Correspondence to*: Felix Ng (f.ng@sheffield.ac.uk)

**Abstract.** A theory of vein impurity transport conceived two decades ago predicts that signals in the bulk concentration of soluble ions in ice migrate under a temperature gradient. If valid, it would mean that some palaeoclimatic signals deep in ice cores (signals from vein impurities as opposed to matrix/grain-boundary impurities) suffer displacements that upset their dating and alignment with other proxies. We revisit the vein physical interactions to show that a strong diffusion prevents such signals from surviving into deep ice. It arises because the Gibbs–Thomson effect, which the original theory had neglected, perturbs the impurity concentration of the vein water wherever the bulk impurity concentration carries a signal. Thus no distinct vein signals will reach a depth where their displacement matters; accordingly, the palaeoclimatic concern posed by the original theory no longer stands. Simulations with signal peaks introduced in shallow ice at the GRIP and EPICA Dome C ice-core sites confirm that rapid damping and broadening eradicates their form by two-thirds way down the ice column; artificially reducing the solute diffusivity in water (to mimic partially-connected veins) by $10^3$ times or more is necessary for signals to penetrate into the lowest several hundred metres with minimal loss of amplitude. The deep solute peaks observed in ice cores can only be explained by widespread vein disconnection or a dominance of matrix/grain-boundary impurities at depth (including their recent transfer to veins); in either case, the deep peaks would not have displaced far. Decomposing the vein and matrix impurity contributions will aid robust reconstruction from ion records.

## 1 Introduction

Chemical impurity concentrations in ice cores yield diverse palaeoclimatic information (e.g. Legrand and Mayewski, 1997; Wolff et al., 2006). As with other ice-core proxies, such as stable water isotopes, it is generally hoped that post-depositional modification of signals in such records, which may hamper their interpretation, is minimal. For signals of abrupt or discrete (e.g., volcanic) events, of interest is whether their position and shape record their timing and magnitude faithfully. If, for instance, signals diffuse in the ice, neighbouring peaks may merge as they descend towards the ice-sheet base. Conceivably, a range of physico-chemical processes may distort signals, limiting the resolution and accuracy of the retrievable information.

https://doi.org/10.5194/tc-2020-217
Preprint. Discussion started: 7 September 2020


The Cryosphere Discussions

In a landmark paper, Rempel et al. (2001) proposed a theory to show that signals in the bulk concentration of dissolved ionic impurities – major ions such as $SO_4^{2-}$, $Cl^-$ and $Na^+$ – in the water veins at polycrystalline grain junctions (Nye, 1989; Mader, 1992a,b) migrate against the ice when a temperature gradient is present. Driven by what they term "anomalous diffusion", migration occurs in the direction of rising temperature and displaces signals with minimal distortion, so their apparent age deviates from their true age. Rempel et al. (2001) calculated cumulative signal displacements of ~ 0.1–1 m in the lowest kilometre of the GRIP ice core. Their mechanism can decouple the ion records from other ice-core proxies and cause significant age errors in palaeoclimatic histories, especially in deep ice where temperature increases markedly towards the bed. This has prompted evaluation for signs of anomalous diffusion in some ice-core records (e.g. Tison et al., 2015), and simulation of the migration of specific species (e.g. methane sulphonic acid in firn; Osman et al., 2017). Note that it is non-trivial to infer the absence or amount of migration by comparing the records of signal peaks from different cores, due to uncertainty in depth-age scales, a lack of rigorous independent control of where individual peaks should lie, and spatial inhomogeneity in the atmospheric dispersal and deposition of impurities by environmental events. Some studies contend that signal migration may be limited – and thus the ion records dependable, because solute transport is hindered by disconnections in the vein network (Barnes et al., 2003; Barnes and Wolff, 2004), or because most ionic impurities are located at grain boundaries (Barnes and Wolff, 2004) or in salt micro-inclusions within ice crystals (Ohno et al., 2005), instead of in veins. How extensively ice-core chemical records have been altered by anomalous diffusion is unresolved, despite the relevance of this question to the synchronisation of ice-core age scales (e.g. Severi et al., 2007; Fujita et al., 2015) and the dating of events.

Here we re-examine "Rempel's theory" of vein impurity transport (i.e. Rempel et al., 2001), discovering missing elements in it that change the predicted signal evolution. We find that the relevant processes must cause *diffusion* of signals at rates that threaten their survival in ice cores, whether or not a temperature gradient drives their migration. Hence the theory's implications are radically revised. Our purpose is not to develop the theory to show how it can match observed ion records or be used in reconstructions, but to show the contrary: it conflicts with observations of deep ionic peaks in ice cores. Much of our analytical and numerical work (Sects. 2 & 3) is spent on understanding the origin of the strong diffusion and showing its operation. We also introduce a correction to the signal migration speed. Near the end (Sect. 4) we discuss what the revised theory means for the provenance of the major ionic peaks found in the deep parts of many ice core records.

Following Rempel's framework, we model one ion species ($SO_4^{2-}$ is used in our calculations) and processes below the firn-ice transition only. Impurities at grain boundaries and in the ice matrix are not modelled, although we involve them in the discussion. Chemical alteration of signals via cation–anion associations (e.g. Iizuka et al., 2004; Traversi et al., 2009), reaction of vein impurities with dust (Barnes and Wolff, 2004), the segregation of impurities to locations outside veins and thermodynamic coupling between multiple ion species (see the companion papers by Rempel et al. (2002) and Rempel and Wettlaufer (2003)), are ignored.

Before plunging into mathematics, we first outline our key finding schematically; see Fig. 1a–d, where $z$ denotes depth. In Rempel's theory, a centimetre/decimetre-scale peak in the bulk solute concentration of the ice, $c_B$, representing a climate

https://doi.org/10.5194/tc-2020-217
Preprint. Discussion started: 7 September 2020


The Cryosphere Discussions

signal, is mirrored by variations in the ice porosity $\phi$ (Fig. 1c, d). This is because $c_B = c\phi$, where $c$, the solute concentration of the vein water, is determined by temperature $T$ through the liquidus. Background temperature gradient in the ice sets up a gentle gradient in $c$, driving downward solute diffusion through the vein network (Fig. 1a). Interestingly, the porosity modulates the solute diffusion flux so that on the trailing (upper) edge of the signal peak, $d\phi/dz > 0$ increases this flux with distance to draw down $c_B$, whereas on the leading (lower) edge of the peak, $d\phi/dz < 0$ reduces the flux with distance to bump up $c_B$. Thus the $c_B$ peak translates. This mechanism is "anomalous" because *solute diffusion* causes the signal to move *without signal diffusion*, i.e., without changing its shape. In their calculations, Rempel et al. (2001) neglected the small effect of the vein-face curvature on the melting point (the Gibbs–Thomson effect), an approximation which they justified in their companion papers (Rempel et al., 2002; Rempel and Wettlaufer, 2003). Then $c$ depends on $T$ only, not on $c_B$. However, we find that when this seemingly reasonable approximation is not made, the $c_B$ signal causes a perturbation on $c(z)$ that drives non-negligible solute diffusion away from the peak (Fig. 1b), owing to the short length-scale of the signal. Consequently, the $c_B$ peak experiences pronounced broadening and amplitude reduction. In an ice core, these conspire with vertical compression to regulate the evolving peak shape.

Besides Rempel et al. (2001), Barnes et al. (2003) have modelled vein-mediated evolution of dissolved ion signals below the firn-ice transition. Their main interest was to explain the signal diffusion found in the top 350 m of the EPICA Dome C ice core (EPICA community members, 2004), which they inferred from observed trends of peak broadening and damping in the sulphate and chloride records with age. To explain the signal diffusivities estimated for these ions – respectively, $4.7 \times 10^{-8}$ $m^2\ yr^{-1}$ and $2 \times 10^{-7}$ $m^2\ yr^{-1}$, they conceived two models of vein solute transport driven by grain growth, motivated by the fact that the mean grain size in their stretch of the core increases with depth. One model invokes local gradients in $c$ induced by porosity change during spatially non-uniform normal grain growth; this mechanism requires the presence of grain-size variations at the length scale of the $c_B$ signals. The other, an analogue model, uses a cell-based simulation to demonstrate how the disconnection of veins by grain growth (modelled as random removal of cells, and relocation of their impurity to neighbouring cells) causes diffusion even when the vein network is only partially connected. Both models predict no diffusion of $c_B$ unless there is net grain growth.

We do not incorporate the Barnes et al. (2003) mechanisms into our model here, as the "Gibbs–Thomson diffusion" is much faster than their diffusion (by an order of magnitude at least), and adding the latter merely strengthens our conclusions. Our mechanism is independent of grain growth also; it occurs in regions of constant grain size. We do, however, account for the continual motion of veins during grain boundary migration, which causes a slow "residual diffusion" on $c_B$. This mechanism does not require temperature gradient or grain-size variations to operate, and is unaffected by vein disconnection.

https://doi.org/10.5194/tc-2020-217
Preprint. Discussion started: 7 September 2020


## 2 The model

### 2.1 Key relationships

We treat polycrystalline ice in a continuum description with variables as functions of position $\mathbf{x} = (x, y, z)$ and time $t$. Ice with the mean grain size $d_g$ (grain diameter) has the vein length density

$$l \approx \frac{3}{d_g^{\,2}}; \tag{1}$$

we adopt equality in this expression herein. If the vein faces have the radius of curvature $r_v$ (Fig. 1e; Nye, 1989), then the ice porosity $\phi$ is

$$\phi = \alpha r_v^{\,2} l\,, \tag{2}$$

where $\alpha = 0.0725$ is a geometrical factor (Nye, 1991; Mader, 1992a,b). As mentioned before, $c$ is the solute concentration of the vein water, and $c_B$ is the bulk solute concentration of the ice. Recalling

$$c_B = \phi c\,, \tag{3}$$

and using (1) and (2), leads to

$$\frac{d_g^{\,2} c_B}{3\alpha} = c r_v^{\,2}\,. \tag{4}$$

For ice at a temperature $T$ below the reference temperature $T_0$, thermodynamic equilibrium between ice and vein water means that the liquidus relation is satisfied:

$$T_0 - T = \theta_c + \frac{\gamma T_0}{\rho_i L r_v} + \theta_p\,. \tag{5}$$

This equation features in earlier studies of the subject (Nye, 1991; Mader, 1992b; Rempel et al., 2001, 2002; Rempel and Wettlaufer, 2003; Barnes et al., 2003; Dani et al., 2012). The terms on its right-hand side describe the temperature depressions due to solute, interfacial curvature (the Gibbs–Thomson effect) and pressure, respectively; $\rho_i$ is ice density, $L$ is latent heat, and $\gamma$ is a constant. Table 1 lists constant values used in this paper. For the first term, a linear approximation $\theta_c = \Gamma c$ is valid at temperatures not far below the melting point, e.g. $\Gamma = 4.53$ K M$^{-1}$ for $SO_4^{2-}$. The third term is typically small and may be

https://doi.org/10.5194/tc-2020-217
Preprint. Discussion started: 7 September 2020


115 absorbed into $T_0$ by accounting for glaciostatic overburden. Accordingly, the version of (5) that we use for the present analysis is

$$T_0 - T = \Gamma c + \frac{\gamma T_0}{\rho_i L r_v}, \tag{6}$$

but our simulations in Sect. 3 for specific ice-core sites will use (5), together with detailed nonlinear empirical formulas for $\theta_c$ and $\theta_p$ (Appendix A).

120 Given $d_g$, $T$ and $c_B$, (4) and (6) can be solved for $r_v$ and $c$ (e.g. Barnes et al., 2003). Figure 1f illustrates the solution as the intersection point of two curves. In Rempel's theory, it is argued that under glaciological conditions, a large $r_v$ makes the Gibbs–Thomson term negligible so that $\Gamma c \approx T_0 - T$; then $c(z)$ is dictated by the vertical ice temperature profile (Fig. 1a). This approximation amounts to taking the intersection point in Fig. 1f to lie on the dashed line. However, as shown by Fig. 1f, the exact solution for $c$ does depend on $c_B$ – albeit weakly – for fixed $T$ and $d_g$. This dependence lies at the heart of our "Gibbs–

125 Thomson diffusion". Specifically, when $\gamma T_0/\rho_i L r_v \ll \Gamma c$, a first-order approximate solution of (4) and (6) is

$$\Gamma c \approx (T_0 - T) - \frac{\gamma T_0}{\rho_i L r_v}, \quad \text{where} \quad r_v \approx \sqrt{\frac{c_B {d_g}^2 \Gamma}{3\alpha(T_0 - T)}}, \tag{7}$$

or

$$c \approx \frac{1}{\Gamma}\left[(T_0 - T) - \frac{\gamma T_0}{\rho_i L}\sqrt{\frac{3\alpha(T_0 - T)}{{d_g}^2 \Gamma}}\, {c_B}^{-1/2}\right]. \tag{8}$$

This differs from Rempel's approximation by the $\gamma$ (Gibbs–Thomson) term, which causes $\partial c/\partial c_B > 0$ and a perturbation to

130 appear on $c(z)$ where $c_B(z)$ exhibits a signal (Fig. 1b, d). The rate of signal diffusion stemming from this minute perturbation will be quantified later.

If, instead of (6), the full liquidus relation (5) is analysed, with $\theta_c = f(c)$ being a mildly nonlinear function, then these findings are qualitatively unchanged, and (8) would read $c \approx f^{-1}([\ ])$ with $[\ ]$ as given in (8) except that $f^{-1}(T_0 - T)$ replaces $(T_0 - T)/\Gamma$ in the square root.

135

### 2.2 Porosity, water and solute conservation

The rest of the model is now formulated, for ice deforming with velocity $\mathbf{u} = (u, v, w)$. As the porosity is very small, $\phi \sim 10^{-6}$ << 1, the incompressibility condition $\boldsymbol{\nabla}.\mathbf{u} = 0$ holds. The total transport flux of porosity is $\mathbf{u}\phi - \kappa\boldsymbol{\nabla}\phi$. Here the first term

https://doi.org/10.5194/tc-2020-217
Preprint. Discussion started: 7 September 2020


describes advection by ice. The second (Fickian) term describes a net transport of porosity due to the random, unceasing vein motion that accompanies grain boundary migration. We detail its physical derivation in Appendix B. The diffusivity $\kappa$ is given by

$$\kappa = \frac{K(T)}{3c_1}, \tag{9}$$

where $K = K_0\exp(-Q/RT)$ is the temperature-dependent grain growth rate, $R$ is the gas constant, $Q$ is activation energy, and $c_1 \approx 2$ to 3 (we use 2.5 in our simulations).

Accordingly, porosity conservation is described by

$$\frac{\partial \phi}{\partial t} + \nabla.(\mathbf{u}\phi - \kappa\nabla\phi) = \frac{m}{\rho_i}\ , \tag{10}$$

where the melt rate $m$ accounts for phase change in the ice. This result can also be derived from ice mass conservation.

If $\mathbf{q}$ is the water flux percolating through the vein network, then water mass conservation requires

$$\rho_w\left[\frac{\partial \phi}{\partial t} + \nabla.(\mathbf{q} + \mathbf{u}\phi - \kappa\nabla\phi)\right] = m\,, \tag{11}$$

and we deduce from this together with (10) that

$$\nabla.\mathbf{q} = -(1-r)\frac{m}{\rho_i}\ , \tag{12}$$

where $r = \rho_i/\rho_w \approx 0.91$ is the ratio of ice density to water density.

The solute flux is the total transport due to advection by ice and water flow, molecular diffusion in the vein water, and statistical vein motion: $\mathbf{u}c_B + \mathbf{q}c - D\phi\nabla c - \kappa\nabla c_B$. Here, $D$ is the diffusion coefficient for the impurity in water, and the origin of the last term is as explained in Appendix B. The corresponding solute conservation equation is

$$\frac{\partial c_B}{\partial t} + \nabla.(\mathbf{u}c_B + \mathbf{q}c) = \nabla.(\phi D\nabla c + \kappa\nabla c_B)\,. \tag{13}$$

Following Rempel's theory, we define the "anomalous velocity"

$$\mathbf{u}_c = -D\frac{\nabla c}{c} \tag{14}$$

https://doi.org/10.5194/tc-2020-217
Preprint. Discussion started: 7 September 2020


The Cryosphere Discussions

and use $c_B = \phi c$ to rewrite the $D$-contribution in (13) to derive

$$\frac{\partial c_B}{\partial t} + \nabla.[(\mathbf{u}+\mathbf{u}_c)c_B + \mathbf{q}c] = \nabla.(\kappa \nabla c_B)\,. \tag{15}$$

If both water flux $\mathbf{q}$ and the $\kappa$-term ("residual diffusion" due to vein motion) are ignored, this simplifies, after using the incompressibility condition, to the Rempel et al.'s (2001) equation:

$$\frac{\partial c_B}{\partial t} + (\mathbf{u}+\mathbf{u}_c).\nabla c_B = -(\nabla.\mathbf{u}_c)c_B\,. \tag{16}$$

As is well rehearsed in their theory, the advection term here predicts migration of chemical signals at the velocity $\mathbf{u}_c$ against the ice, with $\mathbf{u}_c$ controlled by the temperature profile via the liquidus and (14). Our analyses are to reveal departures from these predictions.

### 2.3 One-dimensional model

For an ice core beneath a flow divide or summit, where the ice motion is downward ($\mathbf{u}$ = (0, 0, $w$)) and horizontal variations in $\phi$ and $c_B$ are negligible, (10) and (15) become

$$\frac{\partial \phi}{\partial t} + w\frac{\partial \phi}{\partial z} = \frac{m}{\rho_i} + \frac{\partial}{\partial z}\left(\kappa \frac{\partial \phi}{\partial z}\right), \tag{17}$$

$$\frac{\partial c_B}{\partial t} + (w+w_c)\frac{\partial c_B}{\partial z} + \frac{\partial}{\partial z}(qc) = \frac{\partial}{\partial z}\left(\kappa \frac{\partial c_B}{\partial z}\right) - c_B\frac{\partial w_c}{\partial z}\,, \tag{18}$$

where $w_c = -(D/c)\partial c/\partial z$ is the anomalous velocity downward. (18) tracks the evolution of the bulk impurity profile $c_B(z, t)$ and its signals, but the water flux $q$ needs to be found via

$$\frac{\partial q}{\partial z} = -(1-r)\frac{m}{\rho_i}\,, \tag{19}$$

with $m$ calculated from (17). This problem is supplemented by (4) and (5) (or (6)), which give the instantaneous distributions of $c$ and $\phi$ from the depth profiles of $c_B$, $T$ and $d_g$. There are five equations ((4), (5), (17)–(19)) for the five unknowns $c_B$, $c$, $\phi$, $q$ and $m$.

https://doi.org/10.5194/tc-2020-217
Preprint. Discussion started: 7 September 2020


The Cryosphere Discussions

### 2.4 Correction to the signal migration velocity

Here we explain the first departure from Rempel's original predictions: the migration speed will be faster than $w_c$, because of water percolation induced by the migration. To see this, we need to put all advective parts of (18) (notably $\partial(qc)/\partial z$) in terms of $c_B$. Let $c(z)$ be time-invariant as in Rempel's theory, and ignore the $\kappa$-term (vein motion), to write (18) as

$$c\left(\frac{\partial \phi}{\partial t}+\frac{\partial q}{\partial z}\right)+(w+w_c)\frac{\partial c_B}{\partial z}=-c_B\frac{\partial w_c}{\partial z}-q\frac{\partial c}{\partial z}\ .$$

Substituting for $\partial q/\partial z$ from (19), using (17) for $m$, converts this to

$$r\left(\frac{\partial c_B}{\partial t}+w\frac{\partial c_B}{\partial z}\right)+w_c\frac{\partial c_B}{\partial z}=-c_B\frac{\partial w_c}{\partial z}-q\frac{\partial c}{\partial z}-(1-r)w\phi\frac{\partial c}{\partial z}\ . \qquad (20)$$

The $z$-derivatives on the left-hand side describe signal advection by ice flow and anomalous diffusion, respectively. Following the scaling argument in the Supplementary Information of Rempel et al. (2001), all terms on the right, based on the background gradient in $c$ (Fig. 1a), are negligible on the length scale of climatic signals ($\lesssim 10^{-1}$ m). In (20), the prefactor $r$ of the time derivative means that the migration speed is $w_c/r$, which exceeds $w_c$ by $\approx 10\%$.

What causes this correction? As introduced in Sect. 1, a migrating $c_B$ peak is mirrored by a moving variation in porosity. This evolution implies freezing and melting on the peak's trailing edge and leading edge (Fig. 1c), causing water to be expelled from and absorbed into these regions, respectively, owing to the density change during phase change (see (19)). Hence a water flow localised about the peak transports solute in the same direction to speed up its migration. Although modest in size, the correction applies at all depths and also in the three-dimensional model.

### 2.5 Diffusion of impurity signals

The second (more crucial) departure from Rempel's predictions is that signals in $c_B$ will diffuse, as we emphasised at the outset. In Rempel's theory, $c_B$ signals suffer no distortion as they migrate under anomalous diffusion except for a slight amplitude change due to the right-hand side of (16). But as anticipated in Sect. 2.1, they will perturb $c(z)$ to drive solute diffusion (Fig. 1). The consequence can be studied via a stripped-down version of (16) where ice flow, water flow and vein motion (residual diffusion) are all ignored:

$$\frac{\partial c_B}{\partial t}+\nabla.(\mathbf{u}_c c_B)=0\,. \qquad (21)$$

https://doi.org/10.5194/tc-2020-217
Preprint. Discussion started: 7 September 2020


The Cryosphere Discussions

For the anomalous velocity, substituting for $c$ from (8) into (14) yields, after some algebra,

$$\mathbf{u}_c = -D\frac{\nabla c}{c} \approx \frac{D}{(T_0 - T)}\left[\nabla T - \frac{\gamma T_0}{2\rho_i L}\sqrt{\frac{3\alpha(T_0 - T)}{d_g{}^2\Gamma}}c_B{}^{-3/2}\nabla c_B\right]. \quad (22)$$

Thus (21) becomes

$$\frac{\partial c_B}{\partial t} + \nabla.\left(\frac{D\nabla T}{T_0 - T}c_B\right) = D\frac{\gamma T_0}{2\rho_i L}\sqrt{\frac{3\alpha}{d_g{}^2\Gamma}}\nabla.\left(\frac{c_B{}^{-1/2}\nabla c_B}{\sqrt{T_0 - T}}\right). \quad (23)$$

This partial differential equation implies not only signal migration driven by $\nabla T$, but also signal diffusion, due to the right-hand (Gibbs–Thomson) term, which encapsulates the $c$-perturbation. The diffusion is nonlinear and independent of $\nabla T$. Both the diffusion and advection terms in (23) are controlled by $D$ because they originate from the molecular diffusion of solute in vein water. Setting $\gamma \to 0$ (which forces $\Gamma c \equiv T_0 - T$) recovers Rempel's theory.

How fast do signals diffuse? One way to gauge their rate of (diffusional) broadening and damping versus migration is by taking the magnitude ratio of the terms in the square bracket in (22):

$$\chi = \frac{\gamma T_0}{2\rho_i L}\sqrt{\frac{3\alpha(T_0 - T)}{d_g{}^2\Gamma}}c_B{}^{-3/2}\frac{|\nabla c_B|}{|\nabla T|}. \quad (24)$$

The dimensionless number $\chi$, which also sizes diffusion against advection in (23), resembles the inverse of the Péclet number in fluid mechanics. But the context here is unique as our model concerns the transport of bulk concentration signals, and the underlying physics involve the geometry of the vein network and two-phase (solute–ice) thermodynamic equilibrium.

As an example, taking $T_0 - T \sim 25$ K, $|\nabla T| \sim 20$ K/km = 0.02 K m$^{-1}$, $d_g \sim 5$ mm, $c_B \sim 1$ $\mu$M and $|\nabla c_B| \sim 1$ $\mu$M/10 cm = $10^{-5}$ M m$^{-1}$ (a decimetre-scale signal), which roughly approximate conditions in the lower third of the GRIP and EPICA ice cores, gives $\chi \sim 1.7$. The effective diffusivity in the right-hand term of (23) is then $2.1 \times 10^{-6}$ m$^2$ yr$^{-1}$, which is much higher than the diffusivities reported by Barnes et al. (2003) (Sect. 1). Although our ballpark estimates here depend on the chosen values (they also vary with the signal magnitude, $c_B$) and will change if we consider elsewhere in the ice column, they show that diffusion can pervasively modify signals, whose short length scales play a key role in amplifying the perturbations on $c$ to cause diffusion at a rate rivalling migration. We confirm this by numerical simulation next.

https://doi.org/10.5194/tc-2020-217
Preprint. Discussion started: 7 September 2020


The Cryosphere Discussions

## 3 Ice-core numerical experiments

Using the model above, which revises and extends Rempel's theory, we proceed to simulate the distortion of impurity signals in ice cores in both Greenlandic and Antarctic settings, by doping shallow ice with chemical peaks and seeing how they evolve. Most experiments explore predictions with a fully-connected vein network, but we include some that simulate partial disconnections ("blocked veins") by decreasing the molecular diffusivity $D$.

### 3.1 Material reference frame and set-up

A general simulation of (4), (5) and (17)–(19) would couple them to time-varying velocity, temperature and grain-size distributions in the ice column. But while the corresponding ice flow and thermal calculations are well established (e.g. Cuffey and Paterson, 2010), reliable grain-size modelling remains out of reach, especially for deep ice, where the way in which the mean grain size $d_g$ is governed by strain-induced recrystallisation processes is poorly understood (Faria et al 2013; Ng and Jacka 2014). Consequently we prescribe time-invariant "background" profiles of $w(z)$, $T(z)$ and $d_g(z)$ in our experiments.

We track signals in a reference frame moving with the ice, because their length scale ($\lambda \lesssim 10^{-2}$ m) is much shorter than the core (ice thickness $H \sim 10^3$ m). The computational burden of modelling a short ice section rather than the whole core is also substantially less. To measure the separation distance of signals from ice of age $t$, we use the displacement variable $z' = z - g(t)$, where $g(t)$ is the core's depth-age scale, defined by

$$t = g^{-1}(\zeta) = \int_0^{\zeta} \frac{dz}{w(z)} . \tag{25}$$

The change of variable from $z$ to $z'$ involves $\partial/\partial z \to \partial/\partial z'$ and $\partial/\partial t \to \partial/\partial t - g'(t)\partial/\partial z'$, with $g'(t) \equiv w(g(t))$, so (17) and (18) become

$$\frac{\partial \phi}{\partial t} + \tilde{w}\frac{\partial \phi}{\partial z'} = \frac{m}{\rho_i} + \frac{\partial}{\partial z'}\left(\kappa \frac{\partial \phi}{\partial z'}\right) , \tag{26}$$

$$\frac{\partial c_B}{\partial t} + \tilde{w}\frac{\partial c_B}{\partial z'} + \frac{\partial}{\partial z'}(qc) = \frac{\partial}{\partial z'}\left(\kappa \frac{\partial c_B}{\partial z'}\right) - c_B \frac{\partial w_c}{\partial z'} , \tag{27}$$

with the ice velocity in the new reference frame $\tilde{w}$ given by

$$\tilde{w}(z',t) = w(g(t) + z') - w(g(t)) . \tag{28}$$

This is the velocity field at time $t$ seen from the (moving) ice at depth $g(t)$. Figure 2 depicts characteristic curves representing material trajectories on the $z$–$t$ and $z'$–$t$ plots under the typical compressive flow at a divide, where $-dw/dz$ is the vertical strain

https://doi.org/10.5194/tc-2020-217
Preprint. Discussion started: 7 September 2020


255 rate. As a signal descends, layer-thinning causes it to narrow, but this is countered by our newly-discovered Gibbs–Thomson diffusion and residual diffusion, while anomalous diffusion displaces it from the ice if the temperature gradient is non-zero.

To derive a self-contained evolution equation for $c_B$, we combine (27), (26) and (19) by using the same substitutions as those leading to (20), finding

$$r\left(\frac{\partial c_B}{\partial t}+\tilde{w}\frac{\partial c_B}{\partial z'}\right)+w_c\frac{\partial c_B}{\partial z'}=-c_B\frac{\partial w_c}{\partial z'}+\frac{\partial}{\partial z'}\left(\kappa\frac{\partial c_B}{\partial z'}\right)-q\frac{\partial c}{\partial z'}-(1-r)\left[\phi\left(\frac{\partial c}{\partial t}+\tilde{w}\frac{\partial c}{\partial z'}\right)+c\frac{\partial}{\partial z'}\left(\kappa\frac{\partial \phi}{\partial z'}\right)\right]. \quad (29)$$

260 The terms on the right-hand side here involving $c$ and $\phi$ are negligible, as scaling shows that they are $\sim \lambda(1–r)/H \sim 10^{-6}$ times of those terms on the left. This is verified numerically in all of our experiments. Therefore we approximate (29) as

$$r\frac{\partial c_B}{\partial t}+(r\tilde{w}+w_c)\frac{\partial c_B}{\partial z'}=-c_B\frac{\partial w_c}{\partial z'}+\frac{\partial}{\partial z'}\left(\kappa\frac{\partial c_B}{\partial z'}\right). \quad (30)$$

In our simulations, (30) is solved by the explicit finite-difference method, with the anomalous velocity computed from $w_c = -(D/c)\partial c/\partial z$ (Appendix A details the solution for $c$ from (4) and (5)), the diffusivity $\kappa$ calculated from (9), and $\partial c_B/\partial z = 0$ 265 prescribed at the $z'$-domain boundaries (this leads to no evolution there), far from the signal of interest. The doped signal is introduced at a depth near the firn-ice transition ($\approx$ 100 m), in ice whose age $t$ corresponds to that depth. The subsidiary variables $\phi$, $r_v$, $m$ and $q$ are also calculated from $c$ and $c_B$ at each time step. Rempel et al. (2001) argued that $|c_B(\partial w_c/\partial z)| \ll |w_c(\partial c_B/\partial z)|$, but we do not ignore the term $-c_B(\partial w_c/\partial z')$ on the right-hand side of (30), because the full flux divergence $\partial(w_c c_B)/\partial z'$ is needed for solute conservation, i.e., no leakage.

270 We experiment with two sets of background profiles (Fig. 3), based on the glaciological conditions at the GRIP ice core site in central Greenland and the EPICA Dome C core site in Antarctica. In the GRIP runs, we use the depth-age scale $t(z)$ and velocity $w(z)$ from a Dansgaard-Johnsen model with the ice thickness $H$ = 3029 m, the kink at 1000 m above the bed, and surface accumulation rate $a$ = 0.23 m a$^{-1}$ ice equivalent. In the EPICA runs, we use $t(z)$ and $w(z)$ from the model $w = m + (a – m)[(H – z)/H)]^n$ (Ritz, 1992) with $H$ = 3275 m, $n$ = 1.7, $a$ = 0.023 m a$^{-1}$ and the basal melt rate $m$ = 0.0008 m a$^{-1}$, which yields 275 a depth-age scale approximating the one published by Parrenin et al. (2007). Smoothed versions of $T(z)$ and $d_g(z)$ measured at the ice-core sites are used (Fig. 3c–d, 3g–h). The prescribed profiles are exemplative only. In reality, ice at different depths has experienced different glaciological conditions due to changing accumulation, ice-sheet elevation and climatic temperature over interglacial–glacial timescales. Our interest is not in reconstructing the histories of these conditions.

https://doi.org/10.5194/tc-2020-217
Preprint. Discussion started: 7 September 2020


280

### 3.2 Results: single-peak experiments

Figure 4a presents snapshots from a GRIP run of the evolution of a decimetre-scale signal doped as a Gaussian peak (grey curve: $c_B = 1 + 5\exp[-(z'/\Delta)^2]$, with $\Delta = 0.08$ m) in ice 500 years old ($z = 112.4$ m). Initially the peak, centred at $z' = 0$, has a "full width at half maximum" (FWHM) of 0.13 m. Its set amplitude, 5 $\mu$M, is based on the size of commonly observed peaks

285 in ice-core records (e.g. $\sim 600$ $\mu$g $L^{-1}$ for $SO_4^{2-}$; $\sim 150$ $\mu$g $L^{-1}$ for $Cl^-$; $\sim 80$ $\mu$g $L^{-1}$ for $Na^+$). The peak decays rapidly in the first 20 kyr (upper 2 km at the GRIP site) with negligible migration, and migrates into $z' > 0$ more noticeably afterwards, as the ice section descends deeper where the temperature gradient increases (Fig. 3c). Movie S1 shows the full evolution of this control run. Strong diffusion of the signal is evident not just from the peak's decay, but also its broadening, which overcomes the effect of vertical compression. Recall that in the material reference frame, compression shortens the section continually,

290 so ice enters the simulation domain at both ends. Figs. 4b and c exemplify the perturbation on $c$ (caused by the $c_B$ peak) and the resulting large wiggle on the velocity $w_c$, which represents the $\gamma$-contribution in (22) and is what causes the Gibbs–Thomson diffusion. As in Rempel's theory, the signals on $\phi$ and $r_v$ are collocated with the $c_B$ peak throughout the evolution.

To check this diagnosis for the origin of signal diffusion, another run is conducted (Fig. 4d–f; Movie S1) with everything unchanged except that the Gibbs–Thomson term in (5) is turned off by setting $\gamma = 0$. As expected, the strong diffusion in the

295 control run disappears, as no perturbation now arises on $c$ and $w_c$, but there is still residual diffusion from vein motion. The peak narrows under vertical compression without much amplitude reduction until $t \approx 20$ kyr. It subsequently decays because strong $c_B$ gradients on its steepening sides amplify the residual diffusion, despite $\kappa$ being small ($\sim 10^{-8}$ $m^2$ $yr^{-1}$; Fig. B2). The peak's migration trajectory in this run is identical to that in the control run because migration is independent of the peak shape and the diffusion mechanisms. By $t \approx 100$ kyr ($\approx 2800$ m depth) it has displaced from the ice by $\approx 0.6$ m. A further experiment

300 with $\kappa = \gamma = 0$ (not shown) reproduces the "Rempel limit" of a migrating peak with no diffusion, as far as its diminishing width can be resolved by our $z'$-grid spacing, 0.0025 m. This imples that the simulated signal behaviour in the experiments is not due to numerical diffusion in our finite-difference scheme. Finally, repeating the control run with $\kappa = 0$ modifies the results in Fig. 4a only slightly, confirming that residual diffusion becomes important only when a signal becomes very narrow.

Figure 5a–c and Movie S2 present the control run for EPICA, where ice 4 kyr old ($z = 89.9$ m) is doped with the same

305 peak. The simulated behaviour is similar to that in the GRIP run, but occurs on a much longer timescale due to the low accumulation rate at the EPICA site. The peak migrates from the start because a sizeable temperature gradient spans the ice column (Fig. 3g). Low compressive strain rate, coupled with slow ice submergence and long time for diffusion, yields a wider

https://doi.org/10.5194/tc-2020-217
Preprint. Discussion started: 7 September 2020


peak at all depths than in the GRIP run that has a vastly increased "age span" (i.e., the peak's width in the age domain; discussed later in Fig. 7c, f) compared to the doped signal. Again, comparison against a run with $\gamma = 0$ (Fig. 5d–f; Movie S2) confirms the Gibbs–Thomson perturbation as the cause of signal damping and broadening, and illustrates the weaker residual diffusion.

The rapidity of signal widening versus migration in distorting the peak in both control runs (Figs. 4a and 5a) is anticipated by the non-small dimensionless number $\chi$ in Sect. 2.5. According to (24), near-constant temperature in the top half of the GRIP column (Fig. 3c) preconditions a large $\chi$ there. Indeed, signal diffusion dominates that part of the GRIP control run, confirming also its independent operation from migration. Deeper in both cores, migration becomes more significant as $\chi$ is reduced by higher $T$ and d$T$/d$z$. Grain-size variations also influence the simulated signal decay, with large $d_g$ near the bed (Fig. 3d, h) slowing its rate in theory, but the peaks in our control runs have long dissipated before reaching such depths.

These initial runs demonstrate the signal migration of Rempel's theory, but paradoxically highlight that signals may not survive deep into the ice where it predicts their displacement to become large to be palaeoclimatically important. More precisely, some remnant signals always survive, but with such small amplitudes and such large age spans compared to the original signals that all essential palaeoclimatic information has been lost. There is an apparent problem to resolve, as distinct deep ionic peaks are found in some ice cores (e.g. Mayewski et al., 1997; Mayewski, 1999; Traversi et al., 2009; Tison et al., 2015), although they may be due to impurities outside veins.

Sticking with the vein model for now, can peaks with a different shape survive damping and broadening to reach deep ice? We study this by changing the width of the doped peaks, as this alters their flank gradient, which is a key control of their diffusion rate. Sensitivity experiments are conducted by varying the width parameter $\Delta$ of the Gaussian function between 0.02 and 0.32 m (with the control run parameters unchanged), and by tracking the amplitude, FWHM (full width at half maximum) and age span of the peak in each simulation. The age span is found by dividing the FWHM by the local ice velocity $w$.

Figures 6 and 7 plot – for GRIP and EPICA, respectively – the evolving peak morphometry in these "$\Delta$ experiments" (grey curves). The control runs (black) and the runs where the Gibbs–Thomson effect has been turned off (orange) are included for comparison. As shown by the grey curves, doping a narrower initial peak hampers its survival, as its steep sides cause strong diffusional draw-down of amplitude; broader peaks retain amplitude for longer but meet the same fate as they narrow under vertical compression. We observe interesting feedback between width and amplitude evolution. Compression steepens the flanks of signals to accelerate their damping, whereas amplitude reduction makes them shallower and less prone to damping and broadening. Thus the compressive strain rate is a key driver of signal diffusion. The balance of compression and broadening causes different peaks to end on similar width trajectories at depth (panels b & e, Figs. 6 and 7). Accordingly, peaks with different initial durations acquire near-equal age spans increasing down core (panels c & f, Figs. 6 and 7), which define the minimum time resolution for deep climate signals. These interactions are absent from the study by Rempel et al. (2001), who did not simulate signal shape evolution; their companion papers (Rempel et al., 2002; Rempel and Wettlaufer, 2003) did so but excluded layer-thinning and diffusion.

https://doi.org/10.5194/tc-2020-217
Preprint. Discussion started: 7 September 2020


So, can single peaks survive into deep ice? The Δ experiments show that peaks at decimetre/centimetre scale struggle to do so. Even for initially wide peaks (e.g. Δ = 0.32 m) near the firn-ice transition, the Gibbs–Thomson diffusion has reduced their amplitude four-fold by the time they reach $z \approx 2300$ m at GRIP (where the age is ≈ 25 ka), and 2000 m at EPICA (≈ 175 ka). Setting $\gamma = 0$ prolongs the signals' survival (Figs. 4–7), but residual diffusion still prevents them from reaching the lowest several hundred metres with a sizeable fraction of their original amplitude, not to mention that ignoring the Gibbs–Thomson effect is unphysical.

In the present theoretical framework, is there any way for signals to reach deep ice without losing integrity (amplitude, narrowness)? One possibility is the suppression of solute transport by partial vein blockage/disconnection, which we simulate here in a crude manner by artificially decreasing the molecular diffusivity $D$ – this cannot capture heterogeneous vein transport at the grain scale. In Figs. 6 and 7, the blue curves plot the results of simulations with $D$ suppressed by different factors. The same doped peak and parameters of the control runs are used otherwise. A suppression factor of 0.001–0.01 postpones signal decay to a similar extent as turning off the Gibbs–Thomson effect. The lesser factor (0.001) allows the peak to reach 2750 m with half its original amplitude. Even with such strong suppression, however, peak survival is hindered in deeper ice because the low strain rate there (Fig. 3b, f) provides ample time for signal diffusion to occur, and rising temperature near the bed increases $\kappa$. Note that in Figs. 6 and 7, a perfectly-preserved peak signal that does not diffuse would have constant amplitude and age span and its FWHM would decrease towards the bed as a result of vertical compression.

The simulated displacement and age offset of the peaks are of palaeoclimatological interest. Figure 8 shows that in the control runs the peaks displace by $\sim 1$ m or more in deep ice, causing their apparent age to exceed their true age by hundreds of years in ice ≈ 100 ka at GRIP, and by several thousand years in ice ≈ 400 ka at EPICA. Since the migration rate is independent of the signal shape, the results from the Δ experiments overlap with the control curves. On the other hand, decreasing $D$ suppresses both signal migration and diffusion (see (23)), so the corresponding peaks remain much narrower during their evolution (Figs. 6 and 7, b & e) and migrate much less than in the control runs (Fig. 8a–d, numbered curves). A suppression factor of 0.001–0.01 enables a peak with FWHM < 0.2 m (age span < 200 yr) to reach ≈ 2900 m depth with an age offset of < 50 yr at GRIP and < 300 yr at EPICA. Note that these numerical results, which are mainly illustrative, depend on the depth-age scale assumed for each site, notably its precise behaviour at depth.

For completeness, all of the above experiments have been repeated with doped peaks with twice the amplitude (10 $\mu$M), to cater for some especially high (though relatively rare) peaks in the observed records, which may have more chance to survive. Although the corresponding remnant signals retain greater absolute concentrations at all depths than before, their pattern of decay relative to the initial amplitude and the FWHM and age span results are altered only marginally (Figs. S1 and S2 – see Supplement; cf. Figs. 6 and 7). Thus it remains difficult for palaeoclimate information to be preserved at depth.

https://doi.org/10.5194/tc-2020-217
Preprint. Discussion started: 7 September 2020


370

### 3.3 Results: multiple-peak experiments

The diffusion of $c_B$ means that neighbouring peaks can merge as they descend the ice column. This process is illustrated in Figure 9 and Movie S3 by a simulation with two peaks. Such merging suggests a second explanation for why distinct peaks can feature in deep ice even with strong damping: instead of deriving from a single peak high up in the column, a deep peak
375 may form by the agglomeration of multiple signals/peaks as these merge under compression. This signal-forming mechanism may not be evident from the $c_B$ profile measured from ice cores, which provides an instantaneous record of the signals.

To test this idea, in our final experiments we simulate the evolution of multiple signals doped in shallow ice stretches 20 m long at GRIP and 80 m long at EPICA. Three runs are made for each site, one with the control-case parameters and two with $D$ suppressed by 0.1 and 0.03 (to simulate vein blockage), with both the Gibbs–Thomson effect and residual diffusion
380 included, and using an initial $c_B$ profile formed by adding many Gaussian peaks (numbering 300 at GRIP and 1200 at EPICA) of random amplitudes, widths and positions onto a 1 $\mu$M base level (Fig. 10a). Movies S4 and S5 document these runs.

We focus our analysis on the EPICA runs (Fig. 10; Movie S5), as the GRIP findings are qualitatively similar (although things occur faster there). In the control run (black curves), strong damping and merging smooth the signals rapidly, so $c_B(z')$ retains long-scale variations only – and no peaks – at depth. This outcome is consistent with what we learned from the single-
385 peak experiments. When $D$ is reduced (blue and red curves), compressional shortening, with the now slower diffusion, causes bundle of peaks to merge into new signals that subsume their solute content. This process operates continuously on all signals, with stretches having a high density of peaks turning into peaks, and stretches having a low density into troughs. The vertical compression is crucial in helping signals maintain their integrity against diffusion.

When $D$ is suppressed by 0.03 (Fig. 10, red curves), we see distinct peaks persisting in deep ice, many of them traceable
390 back in time to predecessor groups of peaks, rather than a single peak (e.g. see dashed boxes). The balance of diffusion and shortening here is such that the deep peaks have similar widths as their shallow counterparts ($\sim$ dm), despite an overall reduction of signal amplitude with depth. The ice in Fig. 10d has shortened by approximately ten times since the start of the run, so each peak there encapsulates the signals and solute of an original interval some ten times longer. Signal survival here is aided by the enhanced survival of single peaks due to decreased molecular diffusivity (Sect. 3.2), but also involves the
395 lumping of solute from neighbouring peaks. We find in further experiments (not shown) that when $D$ is reduced even more (suppression factor $\lesssim 0.001$), the peaks continue to narrow into the $\sim$ cm range at depth. Fig. 10 shows an effect already known from the single-peak experiments: a decrease in $D$ reduces the displacement as well as broadening of the signals.

The foregoing experiments demonstrate how long-scale averages on $c_B$ at shallow depths – reflecting long-term background levels of impurity input at an ice-core site – evolve to become meaningful variations at depth, as signals are
400 compressed and their fine details filtered out by diffusion. In Fig. 10, the mean level of the 3,600-year long signal sequence is

https://doi.org/10.5194/tc-2020-217
Preprint. Discussion started: 7 September 2020


The Cryosphere Discussions

preserved at depth as a bump (of the same duration) that is ≈ 6 $\mu$M above the surrounding ice. Ice-core analyses of the major ions frequently interpret deep features of this kind as reflecting real palaeoclimatic variations on time scales of $10^1$–$10^2$ kyr (e.g. Mayewski et al., 1997, EPICA community members, 2004); these analyses are intuitively comfortable with an inherent loss of details in deep ice, given the effect of layer-thinning and the finite resolution of ice-core sampling. Our simulations highlight the Gibbs–Thomson effect in vein impurity transport as a possible cause of the low-pass filtering. Importantly, they show that the long-scale signals will migrate under Rempel's anomalous diffusion mechanism unless the vein network is partially disconnected (see the bump's locations in Fig. 10e).

## 4 Discussion and conclusions

For two decades, Rempel's theory has raised concerns that palaeoclimatic signals in the soluble ion records of ice cores may have displaced by anomalous diffusion and suffer large age discrepancies, especially in the older, deeper parts of the records. Objections to signal migration invoke impeded or insignificant solute transport through veins – that the veins are partially disconnected (blocked by solid impurities and bubbles) or that most chemical signals reside outside veins, in the ice matrix or at grain boundaries.

A more fundamental issue with Rempel's theory is explained herein. We showed that while $c_B$ signals can migrate in a connected vein system, a strong Gibbs–Thomson diffusion damps them, preventing decimetre-scale or shorter signals from surviving into deep ice; only much longer background variations can survive to exhibit migration. *As the physics predicts no or few remaining short signals where their displacement matters, the original concern is no longer valid*. In our revised theory, signal damping is aided by a weaker residual diffusion due to stochastic vein motion. Modifying the derivation of this diffusion mechanism (Appendix B) to include accelerated grain-boundary motion during migration recrystallisation in deep ice (Duval and Castelnau, 1995), or accounting for the grain-growth driven diffusion of Barnes et al. (2003) in the model, strengthens this primary conclusion.

The conclusion is unaffected also if we consider multiple solute species interacting via the liquidus curve (Rempel et al., 2002; Rempel and Wettlaufer, 2003). These authors showed that the $c_B$ signals of different species would then line up as they evolve, with periodic signals becoming in phase, and peaks in each species inducing collocated "sympathetic peaks" in other species; these adjustments occur in a time of $\lambda^2/D \sim$ 1–10 yr for short signals ($\lambda \sim 10^{-1}$ m). Reformulating our theory for multiple species would thus add to the outcome an initial fast alignment of signals, before they evolve by the mechanisms studied herein.

What do our findings mean for the integrity and interpretation of ion records from ice cores? And what explains the occurrence of well-defined signal peaks deep in those records? To ponder these, it is useful to start with two end-member scenarios:

https://doi.org/10.5194/tc-2020-217
Preprint. Discussion started: 7 September 2020


The Cryosphere Discussions

*Scenario 1: Vein-dissolved ionic impurities comprise the main contribution to $c_B$, with matrix impurity contributions negligible.* In this scenario, the deep peaks can only be explained by widespread vein disconnection, which we modelled by reducing the molecular diffusivity $D$. The GRIP and EPICA simulations show that the suppression factor on $D$ needs to be $\lesssim 0.001$ for shallow single peaks to survive into depth, but a weaker suppression ($\sim 0.01$) allows some deep peaks to persist via compression-diffusion merging of signals. Relatedly, Figs. 6–8 suggest the possibility of determining the suppression factor from the width, amplitude and position of the deep peaks, and then estimating their age offset. In practice, the unknown initial peak size/shape will introduce uncertainty to this estimation.

This scenario spells good news for palaeoclimatic interpretation. The deep signals would not have displaced far to accrue large age offsets because reduced vein transport limits their migration speed (Fig. 9). However, diffusional merging means that some signals may be a distorted, lumped signature of multiple climate events. The simulated diffusion smooths details more than the low-pass filtering caused by finite resolution of the $c_B$ measurements – typically, $\sim$ 10 cm in traditional ice-core sampling, and $\approx$ 1 cm or less if using Continuous Flow Analysis (Kaufmann et al., 2008; Bigler et al., 2011). At the model ice-core sites, the highest time resolution of climatic information retrievable from $c_B$ is quantified by the depth-dependent age spans in Figs. 6 and 7.

*Scenario 2: Impurities in the ice matrix (e.g. in salt micro-inclusions) and/or at grain boundaries dominate $c_B$*, and their relative immobility explains the presence at all depths of prominent peaks, which experience vertical compression but do not diffuse or migrate by our mechanisms (they may be modified by slow diffusion through ice or along grain boundaries). In this scenario, signals on the minor vein component of $c_B$ will still evolve if the veins are connected – to migrate, decay, broaden and merge into long-scale variations.

The reality might be a mixture of these scenarios, with vein and matrix ionic impurities responsible for different $c_B$ signals and their contributions varying down-core (and between cores). Thus generally a given record may be the sum of an evolved (diffused, migrated) component and a largely unmodified component. Shallow signals could source from both components, as the metamorphism of snow into ice apportions impurities to crystal grains and the premelted liquid. Matrix impurities may dominate deeper, as the vein signals decay. But if grain growth and recrystallisation relocates some matrix impurities to grain boundaries, and hence to the veins, the vein $c_B$ (at any depth) could be continually refreshed. Such impurity transfer has been suggested by some authors (Glen et al., 1977; Alley et al., 1986a; Mulvaney et al., 1988; Rempel et al., 2001) but debated by others (Ohno et al., 2005; Eichler et al., 2019), while it is understood that both the apportioning and transfer depend on the ion species (Wolff et al., 1988). In any case, these considerations caution against interpreting $c_B$ signals directly for palaeoclimatic variations, e.g., as done in volcanic flux reconstructions from $SO_4^{2-}$. Disentangling the vein and matrix impurity components and their history of post-depositional (coupled?) evolution may be necessary for robust reconstruction. Note that our ideas here

https://doi.org/10.5194/tc-2020-217
Preprint. Discussion started: 7 September 2020


The Cryosphere Discussions

do not oppose the view that most/much ionic impurity occurs in the matrix (Ohno et al., 2005), which does not strictly rule out the presence of all vein impurities.

Based on these considerations, we conclude that distinct deep peaks present in a record may indicate (i) matrix impurities dominating $c_B$, or (ii) relevance of both matrix and vein impurity signals, with the latter damped out at depth or preserved by the disconnection of veins, or (iii) a dominance of vein impurities in a disconnected vein network, or in connected veins receiving recent/sporadic impurity input from the matrix. In each case, the peaks would not have migrated or migrated far, although some diffusional merging may occur in (iii). The limited distortion of the peaks inferred in these cases is consistent with the signal replicability observed between nearby ice cores (Wolff et al., 2005; Gautier et al., 2016), and supports the use of $c_B$ records for synchronising ice-core age scales. However, we expect the glaciological conditions at different ice-core sites to cause contrasting distortion. Even if two core sites (fictitiously) receive identical peak signals at the firn-ice transition (there are no differences in atmospheric transport and deposition of the species and in its modification in firn), variations between their $c_B$ records – for the same ion – will result from differences in strain rate, ice temperature, and dust content/bubble density (which affects the degree of vein blockage). Some peaks in one record may be absent or more damped in the other; a group of peaks in one record may appear as a single merged peak in the other record. These variations, which are well known in ice-core studies, impact the identification and matching of peaks and peak sequences.

Much of our discussion has focussed on short-scale signals. On each $c_B$ record, any background variations – on the scale of $10^1$ m or more – deriving from vein ionic impurities can migrate by anomalous diffusion where the vein system is connected. Therefore care is also needed when dating and interpreting such variations, especially deep ones.

As we have modelled only vein impurity transport in this paper, it is beyond our scope to evaluate the $c_B$ compositions of specific ice cores. Also, the present theory is not meant to resolve where ionic impurities reside in glacier ice. Recent investigations of ice-core samples using Raman spectroscopy (Barletta et al., 2012; Eichler et al., 2019) have yielded a varied picture regarding the distribution of vein vs. matrix impurities in ice, with the former authors finding abundant sulphate and nitrate, but the latter inferring a lack of ionic impurities, at triple junctions (i.e. veins). With an extended literature reporting different results on the subject (e.g. see the review parts of the two papers cited above, and Barnes and Wolff (2004)), this state of knowledge suggests that one should not generalise any particular distribution to all ice. Striving to understand the range of processes of impurity movement and segregation and their controls, and how they can lead to different impurity distributions, is more important.

Hopefully, with better understanding in this direction, future research will be able to develop the theory by coupling our solute and porosity evolution equations for the veins with equations for the formation, transport and modification of matrix impurity sites – going beyond a static partitioning of the vein and matrix impurities (Rempel et al., 2002; Rempel and Wettlaufer, 2003). Such an extended theory will help palaeoclimatic studies more directly, in terms of quantifying post-depositional changes of the $c_B$ records, revealing their artefacts, and developing refined palaeoclimatic inversions from them. We know too little at this stage to envision the details, but the theory presumably needs to address a multi-directional transfer of ionic impurities between matrix, grain boundaries and veins. Other foreseeable complications include chemical reactions

https://doi.org/10.5194/tc-2020-217
Preprint. Discussion started: 7 September 2020


and grain-size evolution influenced by impurities. Work that would aid this development includes (i) a systematic study of $c_B$ signals in ice cores that quantifies their depth-varying spectral content, peak density and peak size-/width-frequency statistics, and (ii) controlled laboratory experiments on ice samples to recreate evolving signals for testing the theory.

Finally, our model equations quantify the degradation of vein ionic signals during ice-core storage. The rates of residual diffusion, Gibbs–Thomson diffusion and signal migration (where storage imparts a non-zero temperature gradient through samples) are all minimised at low temperatures, and may be estimated from (9) and (23).

## Appendix A: solving for vein conditions

From Dani et al. (2012), relevant empirical formulas for the temperature depressions $\theta_c$ and $\theta_p$ in (5) (in Kelvin) are

$$\theta_c = k_1 c + k_2 c^2 + k_3 c^3 \quad \text{and} \quad \theta_p = a_1 p + a_2 p^2 , \tag{A1}$$

where $c$ is measured in M, pressure $p$ is in Pa, and the constants are $k_1 = 4.7971$, $k_2 = -1.188$, $k_3 = 0.685$, $a_1 = 7.61 \times 10^{-8}$, $a_2 = 1.32 \times 10^{-16}$. At a depth $z$, we calculate the overburden pressure as $p = \rho_i g z$ without correcting for firn density. Then combining (4) and (5) yields

$$f = (T_0 - T - \theta_p) - k_1 c - k_2 c^2 - k_3 c^3 - \frac{\gamma T_0}{\rho_i L}\sqrt{\frac{3\alpha c}{c_B d^2}} = 0 . \tag{A2}$$

This equation has one positive real root for $c$. We calculate it numerically with Newton's method, choosing $c = (T_0 - T - \theta_p) / k_1$ as the initial guess.

## Appendix B: residual diffusion of $c_B$ and $\phi$

Consider, in polycrystalline ice, a three-dimensional network of veins with random orientations, which, as the grain boundaries migrate, move in random directions (Fig. B1). Here we show that this can cause diffusion of the bulk solute concentration $c_B$ and porosity $\phi$. For simplicity, we assume the vein motion to be isotropic.

As each vein segment migrates, its motion takes along pore space and solute (we ignore vein water flow, ice deformation, and other processes considered in the main model; Sect. 2.2). Transport arises from vein segments moving in myriad directions. Segments with the same size and solute content moving in opposite directions cancel in terms of contribution. A statistical description is needed to calculate the net effect. Suppose their migration velocities $\mathbf{v} = (v_x, v_y, v_z)$ across a given plane (Fig. B1) follow the probability density function $f$, so that the proportion of vein segments with velocity near $\mathbf{v}$ (in an incremental box $dv_x$–$dv_y$–$dv_z$) is

https://doi.org/10.5194/tc-2020-217
Preprint. Discussion started: 7 September 2020


The Cryosphere Discussions

$$f(v_x, v_y, v_z)dv_x dv_y dv_z = F(v)v^2 \sin\theta'\, d\theta' d\phi' dv\,. \tag{B1}$$

The right-hand side puts $d\mathbf{v}$ in spherical coordinates (we dashed the symbols of the polar angle $\theta'$ and azimuth $\phi'$ to distinguish them from $\phi$ and $\theta$). Under isotropic migration, $F$ is a function of speed $v = |\mathbf{v}|$, independent of direction, and one may suppose $F$ decays to 0 as $v \to \infty$. This formulation resembles the kinetic theory of gases, where $F$ is the Maxwell-Boltzmann distribution (Chapman and Cowling, 1953).

Regardless of the exact form of $F$ for veins, their mean migration speed is

$$\bar{v} = \int_0^\infty \int_0^{2\pi} \int_0^{\pi} F(v)v^3 \sin\theta'\, d\theta' d\phi' dv = 4\pi \int_0^\infty v^3 F(v)\, dv\,. \tag{B2}$$

We expect $\bar{v}$ to be similar to the speed of grain boundaries. An estimate for the latter can be found from the normal grain growth law (Gow, 1969; Duval, 1985; Cuffey and Paterson, 2010),

$$\frac{d(d_g^{\,2})}{dt} = K\,, \tag{B3}$$

where $K$ has been defined in Sect. 2.2. Specifically, following to the results of Hillert (1965) and Ng (2016), we let

$$\bar{v} = \frac{K}{c_1 d_g}\,, \tag{B4}$$

where $c_1 \approx 2$ to 3. The assumption of normal grain growth gives a low-end estimate for $\bar{v}$, because strain-induced dynamic recrystallisation can accelerate grain boundary migration (Duval and Castelnau, 1995). On the other hand, impurities and bubbles may reduce grain-boundary mobility (Alley, 1986a; 1986b). In the present formulation, we exclude these complications, as well as anisotropic vein motion resulting from recrystallisation processes. We ignore any influence on $K$ by the solute concentration $c$, because $c$ refers to impurities dissolved in vein water, rather than impurities at grain boundaries.

Next we calculate the transport fluxes. Imagine a region of uniform porosity and uniform mean grain size where the vein network continually evolves. The incremental flux of porosity (vein space) crossing an area $dA$ in the direction perpendicular to the plane is

$$dJ = \phi\, v\cos\theta'\, F(v)v^2 \sin\theta'\, d\theta' d\phi' dv dA\,. \tag{B5}$$

Integrating this over $v \in [0, \infty]$, $\phi' \in [0, 2\pi]$ and $\theta' \in [0, \pi/2]$ (for unidirectional flux; Fig. B1) yields the porosity flux density

$$j = \frac{dJ}{dA} = \phi\pi \int_0^\infty F(v)v^3\, dv = \frac{1}{4}\bar{v}\phi\,. \tag{B6}$$

The same method applied to the bulk solute content $c_B = \phi c$ gives its flux density as

https://doi.org/10.5194/tc-2020-217
Preprint. Discussion started: 7 September 2020


The Cryosphere Discussions

$$j_c = \frac{1}{4}\bar{v}c_B \,. \tag{B7}$$

Given how these macroscopic fluxes originate from microscopic interactions, they are valid on timescales longer than the timescale of vein-crossing events, $\sim d_g/\bar{v}$.

In a uniform region, the fluxes through $dA$ in opposite directions cancel. But if $\phi$ (or $c_B$) varies spatially, a differential flux occurs; diffusion then arises from the vein motion. The net diffusion rate across a plane, say, at elevation $z = z_0$, is found by subtracting the opposite fluxes at a distance $dz$ on either side, $j_+$ at $z_0 - dz$ and $j_-$ at $z_0 - dz$, where $dz$ locates the planes for evaluating the fluxes from continuum properties. We determine $dz$ by using an argument similar to that in the kinetic theory. Moving vein segments merge and reconfigure on distances on the order of the mean grain size, so vein segments arriving at the plane typically come from a distance $\sim d_g$ since their last "collision", which caused them to switch direction and gain or lose solute; $d_g$ is akin to the particle mean free path in the kinetic theory. Accordingly, we choose $dz$ to be the flux-averaged value of the perpendicular distance $d_g \cos\theta'$ :

$$dz = \frac{\int_0^\infty \int_0^{2\pi} \int_0^{\pi/2} d_g \cos\theta' F(v) v^3 \cos\theta' \sin\theta' \, d\theta' d\phi' dv}{\int_0^\infty \int_0^{2\pi} \int_0^{\pi/2} F(v) v^3 \cos\theta' \sin\theta' \, d\theta' d\phi' dv} = d_g \frac{\int_0^{\pi/2} \cos^2\theta' \sin\theta' \, d\theta'}{\int_0^{\pi/2} \cos\theta' \sin\theta' \, d\theta'} = \frac{2d_g}{3} \,. \tag{B8}$$

It follows that the net diffusive transport across the plane is

$$j_{net} = j_+ - j_- = \frac{1}{4}\bar{v}\left.\phi\right|_{z_0 - 2D/3} - \left.\phi\right|_{z_0 + 2D/3} \approx \frac{1}{4}\bar{v}\left(-\frac{4d_g}{3}\left.\frac{\partial\phi}{\partial z}\right|_{z_0}\right)$$

$$= -\frac{\bar{v}d_g}{3}\left.\frac{\partial\phi}{\partial z}\right|_{z_0} \,. \tag{B9}$$

Combining this result with (B4) gives the diffusivity $\kappa = \bar{v}d_g/3 = K(T)/3c_1$, as given in (9) in the text. Figure B2 plots $\kappa$ against temperature. Interestingly, $\kappa$ is independent of $d_g$ because smaller grains cause faster grain boundary migration, but proportionally shorter mean free path for the vein motion.

https://doi.org/10.5194/tc-2020-217
Preprint. Discussion started: 7 September 2020


## Code and data availability

Our MATLAB code and the simulated data of our control runs are archived at doi:10.15131/shef.data.12735191.
Please use https://figshare.com/s/8607e837455c5188c207 during the review stage.

## Supplement link

Movies S1–S5 and Figs. S1–S2 can be accessed via doi:10.15131/shef.data.12739169.
Please use https://figshare.com/s/aa059ab52b73f472f3fd during the review stage.

## Author contribution

F. S. L. Ng designed and performed the study and wrote the paper.

## Competing interests

The author declares that he has no conflict of interest.

## Acknowledgements

I thank A. J. Sole and A. J. Hepburn for helpful comments on the pre-submission manuscript.

## References

Alley, R. B., Perepezko, J. H., and Bentley, C. R.: Grain growth in polar ice: I. Theory, J. Glaciol., 32, 415–424, 1986a.

Alley, R. B., Perepezko, J. H., and Bentley, C. R.: Grain growth in polar ice: II. Application, J. Glaciol., 32, 425–433, 1986b.

Barletta, R. E., Priscu, J. C., Mader, H. M., Jones, W. L., and Roe, C. W.: Chemical analysis of ice vein microenvironments: II. Analysis of glacial samples from Greenland and the Antarctic. J. Glaciol., 58, 1109–1118, doi:10.3189/2012JoG12J112, 2012.

Barnes, P. R. F., Mader, H. M., Röthlisberger, R., Udisti, R., and Wolff, E. W.: The evolution of chemical peak shapes in the Dome C ice core, Antarctica, J. Geophys. Res., 108, 4126, doi:10.1029/2002JD002538, 2003.

Barnes, P. R. F. and Wolff, E. W.: Distribution of soluble impurities in cold glacial ice. J. Glaciol., 170, 311–324, 2004.

Bigler, M., Svensson, A., Kettner, E., Vallelonga, P., Nielsen, M. E., and Steffensen, J. P.: Optimization of high-resolution continuous flow analysis for transient climate signals in ice cores, Environ. Sci. Technol., 45, 4483–4489, doi:10.1021/es200118j, 2011.

https://doi.org/10.5194/tc-2020-217
Preprint. Discussion started: 7 September 2020


Chapman, S., and Cowling, T. G.: The Mathematical Theory of Non-Uniform Gases, Cambridge University Press, London, 1953.

Cuffey, K. M. and Paterson, W. S. B.: The Physics of Glaciers (4th edn.), Butterworth-Heinemann, Oxford, 2010.

Dani, K. G., Mader, H. M., Wolff, E. W., and Wadham, J. L.: Modelling the liquid-water vein system within polar ice sheets as a potential microbial habitat, Earth Planet. Sci. Letts., 333–334, 238–249, doi:10.1016/j.epsl.2012.04.009, 2012.

Durand, G. and Weiss, J.: EPICA Dome C Ice Cores Grain Radius Data, IGBP PAGES/World Data Center for Paleoclimatology, Data Contribution Series No. 2004-039, NOAA/NGDC Paleoclimatology Program, Boulder CO, USA, 2004.

Duval, P.: Grain growth and mechanical behaviour of polar ice, Ann. Glaciol., 6, 79–82, 1985.

Duval, P. and Castelnau, O.: Dynamic recrystallization of ice in polar ice sheets. J. Phys. IV [Paris], 5, 197–205, doi:10.1051/jp4:1995317, 1995.

Eichler, J., Weikusat, C., Wegner, A., Twarloh, B., Behrens, M., Fischer, H., Hörhold, M., Jansen, D., Kipfstuhl, S., Ruth, U., Wilhelms, F., and Weikusat, I.: Impurity Analysis and microstructure along the climatic transition from MIS 6 into 5e in the EDML ice core using cryo-Raman microscopy, Front. Earth Sci., 7:20. doi:10.3389/feart.2019.00020, 2019.

EPICA community members: Eight glacial cycles from an Antarctic ice core, Nature, 429, 623–628. doi:10.1038/nature02599, 2004.

Faria, S. H., Weikusat, I., and Azuma, N.: The microstructure of polar ice. Part II: state of the art. J. Struct. Geol., 61, 21–49, doi:10.1016/j.jsg.2013.11.003, 2014.

Fujita, S., Parrenin, F., Severi, M., Motoyama, H., and Wolff, E. W.: Volcanic synchronization of Dome Fuji and Dome C Antarctic deep ice cores over the past 216 kyr, Clim. Past, 11, 1395–1416, doi:10.5194/cp-11-1395-2015, 2015.

Gautier, E., Savarine, J., Erbland, J., Lanciki, A., and Possenti, P.: Variability of sulfate signal in ice core records based on five replicate cores, Clim. Past, 12, 103–113, doi:10.5194/cp-12-103-2016, 2016.

Glen, J. W., Homer, D. R., and Paren, J. G.: Water at grain boundaries: its role in the purification of temperate glacier ice, Int. Assoc. Hydrogeol., 118, 263–271, 1977.

Gow, A. J.: On the rates of growth of grains and crystals in South Polar firn, J. Glaciol., 8, 241–252, 1969.

Hillert, M.: On the theory of normal and abnormal grain growth. Acta Metall., 13, 227–238, 1965.

Iizuka, Y., Takata, M., Hondoh, T., and Fujii, Y.: High-time-resolution profiles of soluble ions in the last glacial period of a Dome Fuji (Antarctica) deep ice core, Ann. Glaciol., 39, 452–456, 2004.

Johnsen, S. J., Dahl-Jensen, D., Dansgaard, W., and Gundestrup, N.: Greenland palaeotemperatures derived from GRIP bore hole temperature and ice core isotope profiles, Tellus, 47B, 624–629, 1995.

Kaufmann, P. R., Federer, U., Hutterli, M. A., Bigler, M., Schüpbach, S., Ruth, U., Schmitt, J., and Stocker, T. F.: An improved continuous flow analysis system for high-resolution field measurements on ice cores, Environ. Sci. Technol., 42, 8044–8050, doi:10.1021/es8007722, 2008.

Legrand, M. and Mayewski, P.: Glaciochemistry of polar ice cores: a review. Rev. Geophys., 35, 219–243, 1997.


Mader, H. M.: Observations of the water-vein system in polycrystalline ice, J. Glaciol., 38, 333–347, 1992a.

Mader, H. M.: The thermal behaviour of the water-vein system in polycrystalline ice, J. Glaciol., 38, 359–374, 1992b.

Mayewski, P. A., Meeker, L. D., Twickler, M. S., Whitlow, S. I., Yang, Q., Lyons, W. B., and Prentice, M.: Major features and forcing of high-latitude northern hemisphere atmospheric circulation using a 110,000-year-long glaciochemical series, J. Geophys. Res., 102, 26345–26366, 1997.

Mayewski, P. A.: GISP2 Ions: Deep (D) Core (Detailed), PANGAEA, https://doi.org/10.1594/PANGAEA.55533, 1999.

Mulvaney, R., Wolff, E. W., and Oates, K.: Sulphuric acid at grain boundaries in Antarctic ice, Nature, 331, 247–249, 1988.

Ng, F. S. L.: Statistical mechanics of normal grain growth in one dimension: A partial integro-differential equation model, Acta Mater., 120, 453–462, doi:10.1016/j.actamat.2016.08.033, 2016.

Ng, F. and Jacka, T. H.: A model of crystal-size evolution in polar ice masses. J. Glaciol., 60, 463–477, doi:10.3189/2014JoG13J173, 2014.

Nye, J. F.: The geometry of water veins and nodes in polycrystalline ice, J. Glaciol., 35, 17–22, 1989.

Nye, J. F.: Thermal behaviour of glacier and laboratory ice, J. Glaciol., 37, 401–413, 1991.

Ohno, H., Igarashi, M., and Hondoh, T.: Salt inclusions in polar ice core: location and chemical form of water-soluble impurities. Earth Planet. Sci. Lett., 232, 171–178, 2005.

Osman, M., Das, S. B., Marchal, O., Evans, M. J.: Methanesulfonic acid (MSA) migration in polar ice: data synthesis and theory, The Cryosphere, 11, 2439–2462, doi:10.5194/tc-11-2439-2017, 2017.

Parrenin, F., Barnola, J.-M., Beer, J., Blunier, T., Castellano, E., Chappellaz, J., Dreyfus, G., Fischer, H., Fujita, S., Jouzel, J., Kawamura, K., Lemieux-Dudon, B., Loulergue, L., Masson-Delmotte, V., Narcisi, B., Petit, J.-R., Raisbeck, G., Raynaud, D., Ruth, U., Schwander, J., Severi, M., Spahni, R., Steffensen, J. P., Svensson, A., Udisti, R., Waelbroeck, C., and Wolff, E.: The EDC3 chronology for the EPICA Dome C ice core, Clim. Past, 3, 485–497, doi:10.5194/cp-3-485-2007, 2007.

Pol, K., Masson-Delmotte, V., Johnsen, S., Bigler, M., Cattani, O., Durand, G., Falourd, S., Jouzel, J., Minster, B., Parrenin, F., Ritz, C., Steen-Larsen, H. C., and Stenni, B.: New MIS 19 EPICA Dome C high resolution deuterium data: Hints for a problematic preservation of climate variability at sub-millennial scale in the “oldest ice”, Earth Planet. Sci. Lett., 298, 95–103, doi:10.1016/j.epsl.2010.07.030, 2010.

Rasmussen, S. O., Bigler, M., Blockley, S. P., Blunier, T., Buchardt, S. L., Clausen, H. B., Cvijanovic, I., Dahl-Jensen, D., Johnsen, S. J., Fischer, H., Gkinis, V., Guillevic, M., Hoek, W. Z., Lowe, J. J., Pedro, J. B., Popp, T., Seierstad, I. K., Steffensen, J. P., Svensson, A. M., Vallelonga, P., Vinther, B. M., Walker, M. J. C., Wheatley, J. J., Winstrup, M.: A stratigraphic framework for abrupt climatic changes during the Last Glacial period based on three synchronized Greenland ice-core records: refining and extending the INTIMATE event stratigraphy, Quat. Sci. Rev., 106, 14–28, doi:10.1016/j.quascirev.2014.09.007, 2014.

Rempel, A. W. and Wettlaufer, J. S.: Segregation, transport, and interaction of climate proxies in polycrystalline ice, Can. J. Phys., 81, 89–97, 2003.

https://doi.org/10.5194/tc-2020-217
Preprint. Discussion started: 7 September 2020


Rempel, A. W., Waddington, E. D., Wettlaufer, J. S., and Worster, M. G.: Possible displacement of the climate signal in ancient ice by premelting and anomalous diffusion, Nature, 411, 568–571. doi:10.1038/35079043, 2001.

Rempel, A. W., Wettlaufer, J. S., and Waddington, E. D.: Anomalous diffusion of multiple impurity species: Predicted implications for the ice core climate records, J. Geophys. Res., 107, 1–12, doi:10.1029/2002JB001857, 2002.

Ritz, C.: Un modèle thermo-mécanique d'évolution pour le basin glaciaire Antarctique Vostok-Glacier Byrd: Sensibilité aux valeurs des paramètres mal connus, Ph.D. thesis, Laboratoire de Glaciologie et Géophysique de l'Environnement, Université Joseph Fourier, Grenoble, 377 pp., 1992.

Seierstad, I. K., Abbott, P. M., Bigler, M., Blunier, T., Bourne, A. J., Brook, E., Buchardt, S. L., Buizert, C., Clausen, H. B., Cook, E., Dahl-Jensen, D., Davies, S. M., Guillevic, M., Johnsen, S. J., Pedersen, D. S., Popp, T. J., Rasmussen, S. O., Severinghaus, J. P., Svensson, A., Vinther, B. M.: Consistently dated records from the Greenland GRIP, GISP2 and NGRIP ice cores for the past 104 ka reveal regional millennial-scale $\delta^{18}O$ gradients with possible Heinrich event imprint. Quat. Sci. Rev., 106, 29–46, doi:10.1016/j.quascirev.2014.10.032, 2014.

Severi, M., Becagli, S., Castellano, E., Morganti, A., Traversi, R., Udisti, R., Ruth, U., Fischer, H., Huybrechts, P., Wolff, E., Parrenin, F., Kaufmann, P., Lambert, F., and Steffensen, J. P.: Synchronisation of the EDML and EDC ice cores for the last 52 kyr by volcanic signature matching, Clim. Past, 3, 367–374, doi:10.5194/cp-3-367-2007, 2007.

Thorsteinsson, T., Kipfstuhl, J., and Miller, H.: Textures and fabrics in the GRIP ice core. J. Geophys. Res., 102, 26583–26599, 1997.

Tison J.-L., de Angelis, M., Littot, G., Wolff, E., Fischer, H., Hansson, M., Bigler, M., Udisti, R., Wegner, A., Jouzel, J., Stenni, B., Johnsen, S., Masson-Delmotte, V., Landais, A., Lipenkov, V., Loulergue, L., Barnola, J.-M., Petit, J.-R., Delmonte, B., Dreyfus, G., Dahl-Jensen, D., Durand, G., Bereiter, B., Schilt, A., Spahni, R., Pol, K., Lorrain, R., Souchez, R., and Samyn, D.: Retrieving the paleoclimatic signal from the deeper part of the EPICA Dome C ice core, The Cryosphere, 9, 1633–1648, doi:10.5194/tc-9-1633-2015, 2015.

Traversi, R., Becagli, S., Castellano, E., Marino, F., Rugi, F., Severi, M., de Angelis, M., Fischer, H., Hansson, M., Stauffer, B., Steffensen, J. P., Bigler, M., and Udisti, R.: Sulfate spikes in the deep layers of EPICA-Dome C ice core: Evidence of glaciological artifacts, Environ. Sci. Technol., 43, 8737–8743, doi:10.1021/es901426y, 2009.

Wolff, E.W., Mulvaney, R., and Oates, K.: The location of impurities in Antarctic ice, Ann. Glaciol., 11, 194–197, 1988.

Wolff, E. W., Cook, E., Barnes, P. R. F., and Mulvaney, R.: Signal variability in replicate ice cores, J., Glaciol., 51, 462-468, 2005.

Wolff, E. W., Fisher, H., Fundel, F., Ruth, U., Twarloh, B., Littot, G. C., Mulvaney, R., Röthlisberger, R., de Angelis, M., Boutron, C. F., Hansson, M., Jonsell, U., Hutterli, M. A., Lambert, F., Kaufmann, P., Stauffer, B., Stocker, T. F., Steffensen, J. P., Bigler, M., Siggaard-Andersen, M. L., Udisti, R., Becagli, S., Castellano, E., Severi, M., Wagenbach, D., Barbante, C., Gabrielli, P., and Gaspari, V.: Southern Ocean sea-ice extent, productivity and iron flux over the past eight glacial cycles, Nature, 440, 491–496, doi:10.1038/nature04614, 2006.

https://doi.org/10.5194/tc-2020-217
Preprint. Discussion started: 7 September 2020


The Cryosphere Discussions

695

700 **Table 1:** Constants used in this study.

| Symbol | Value | Parameter |
|---|---|---|
| $\alpha$ | 0.0725 | Geometric constant |
| $c_1$ | 2.5 | Geometric constant |
| $D$ | *$5 \times 10^{-10}$ m$^2$ s$^{-1}$ | Solute diffusivity in vein water |
| $\gamma$ | 0.034 J m$^{-2}$ | Surface energy (in the Gibbs–Thomson term in (5)) |
| $\Gamma$ | 4.53 K M$^{-1}$ | Slope of water–$SO_4^{2-}$ liquidus curve, ≈ 0 °C (Dani et al.,2012) |
| $g$ | 9.81 m s$^{-2}$ | Gravitational acceleration |
| $K_0$ | **$1.68 \times 10^7$ mm$^2$ a$^{-1}$ | Grain growth rate constant |
| $L$ | $333.5 \times 10^3$ J kg$^{-1}$ | Latent heat of melting |
| $\rho_i$ | 917 kg m$^{-3}$ | Ice density |
| $\rho_w$ | 1000 kg m$^{-3}$ | Water density |
| $Q$ | 42.4 kJ mol$^{-1}$ | Grain growth activation energy |
| $R$ | 8.314 J K$^{-1}$ mol$^{-1}$ | Gas constant |
| $T_0$ | 0 °C | Reference temperature (melting point at 1 bar) |

* One-third of the molecular diffusivity in water; see Rempel et al. (2001).

** Value derived from Table 3.1 of Cuffey and Paterson (2010), after multiplying by $6/\pi$ to correct for sectioning and stereological effects
705 (Ng and Jacka, 2014)

710

https://doi.org/10.5194/tc-2020-217
Preprint. Discussion started: 7 September 2020


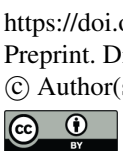



715

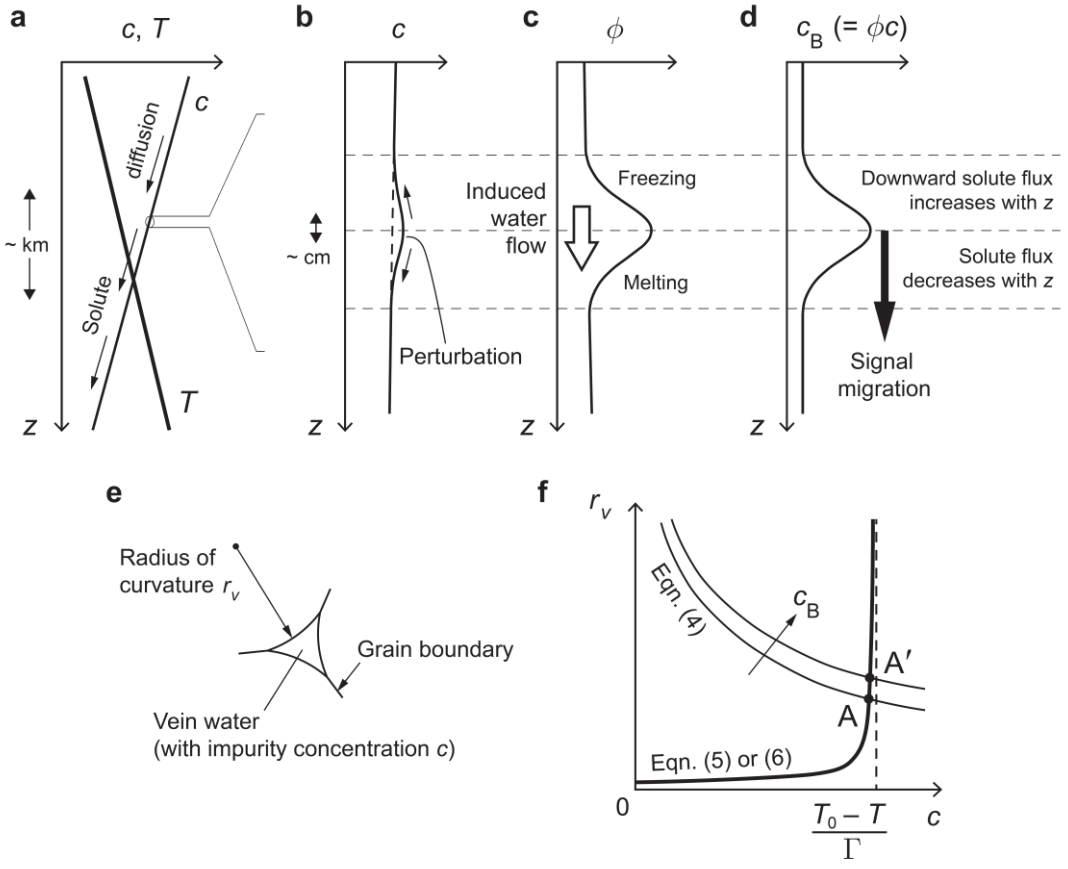


**Figure 1:** Interactions that cause the signal migration mechanism of Rempel et al. (2001) and our signal diffusion mechanism, and variables studied in this paper. (a) Conceptualisation of the vertical profiles of vein impurity concentration $c$ and ice temperature $T$ at the ice-sheet depth scale; $z$ is depth below the ice surface. Panels b to d expand on the short-scale variations around a $c_B$ signal. (b) Vein impurity concentration $c$. (c) Porosity $\phi$. (d) Bulk impurity concentration $c_B$. (e) Vein cross-sectional geometry, showing the definition of the radius of curvature $r_v$. (f) Equilibrium vein conditions as the solution of model equations. An increase in $c_B$ lifts the solution A to A', causing a perturbation on $c$ (see panel b) that drives $c_B$ diffusion. Neglect of the Gibbs–Thomson effect in the theory of Rempel et al. (2001) causes the bold curve in (f) to collapse onto the vertical dash line; then no perturbation arises to diffuse the signal.

https://doi.org/10.5194/tc-2020-217
Preprint. Discussion started: 7 September 2020


The Cryosphere Discussions
Open Access
EGU

730

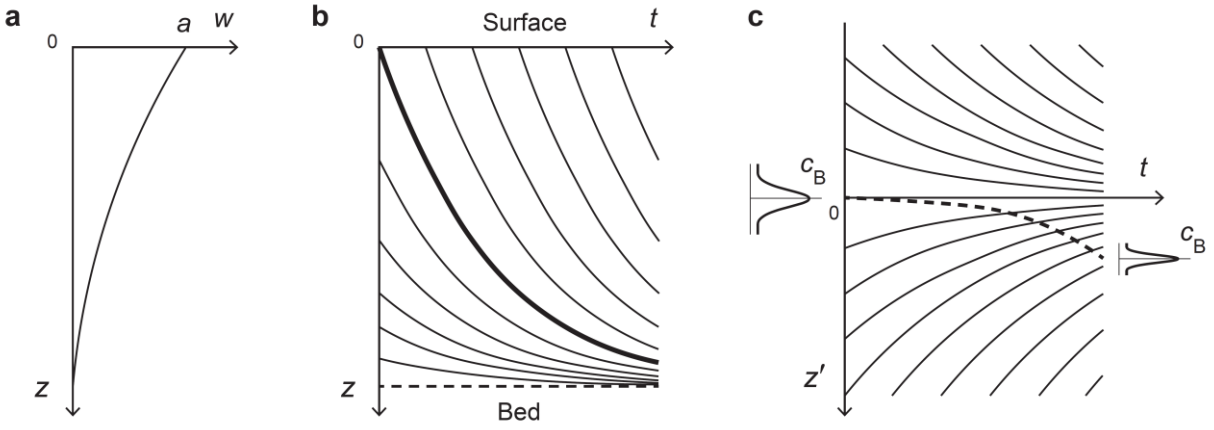


**Figure 2:** (a) Submergence velocity $w(z)$ in an ice core and the corresponding (b, c) $z$–$t$ and $z'$–$t$ plots of material trajectories. The bold line in (b) is the depth-age relation. In (c), $z'$ is a material-following depth coordinate that measures distance from ice at age $t$. An impurity signal centred initially at $z' = 0$ can migrate by anomalous diffusion into $z' > 0$ (dashed curve) and diffuse, while it experiences vertical compression. The $z'$ coordinate system is used in the signal evolution experiments reported in Figs. 4 to 10.

735

740

745

750

https://doi.org/10.5194/tc-2020-217
Preprint. Discussion started: 7 September 2020


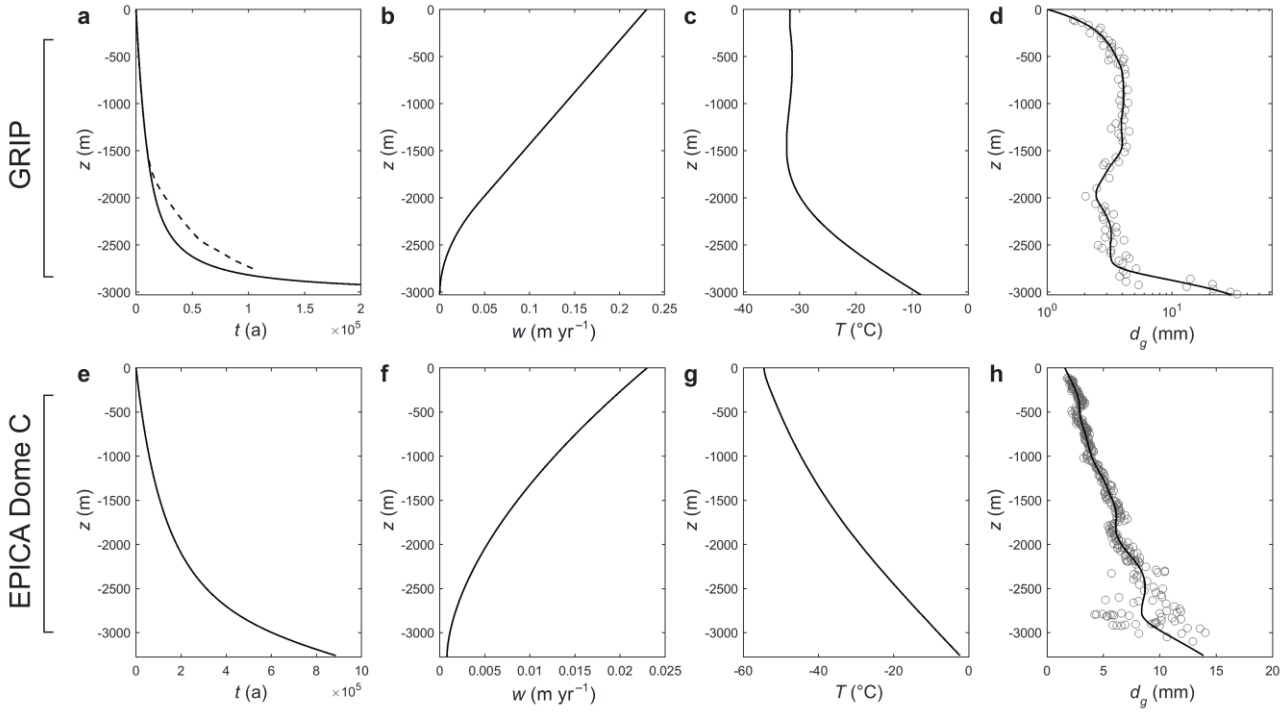


**Figure 3:** Ice-core background fields used in our signal evolution experiments. GRIP ice core: a to d. (a) Age-depth scale and (b) ice velocity from a Dansgaard-Johnsen model. Dashed line in (a) shows the GICC05 modelext timescale (Seierstad et al., 2014; Rasmussen et al., 2014). (c) Ice temperature from Johnsen et al. (1995). (d) Grain-size data from Thorsteinsson et al. (1997) and spline fit used in our modelling. EPICA Dome C core: e to h. (e) Age-depth scale and (f) ice velocity from the model described in Sect. 3.1. (g) Borehole temperature from Pol et al. (2010). (h) Grain-size data from Durand et al. (2004) and spline fit used in our modelling.

https://doi.org/10.5194/tc-2020-217
Preprint. Discussion started: 7 September 2020


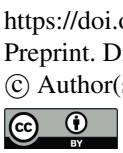



775

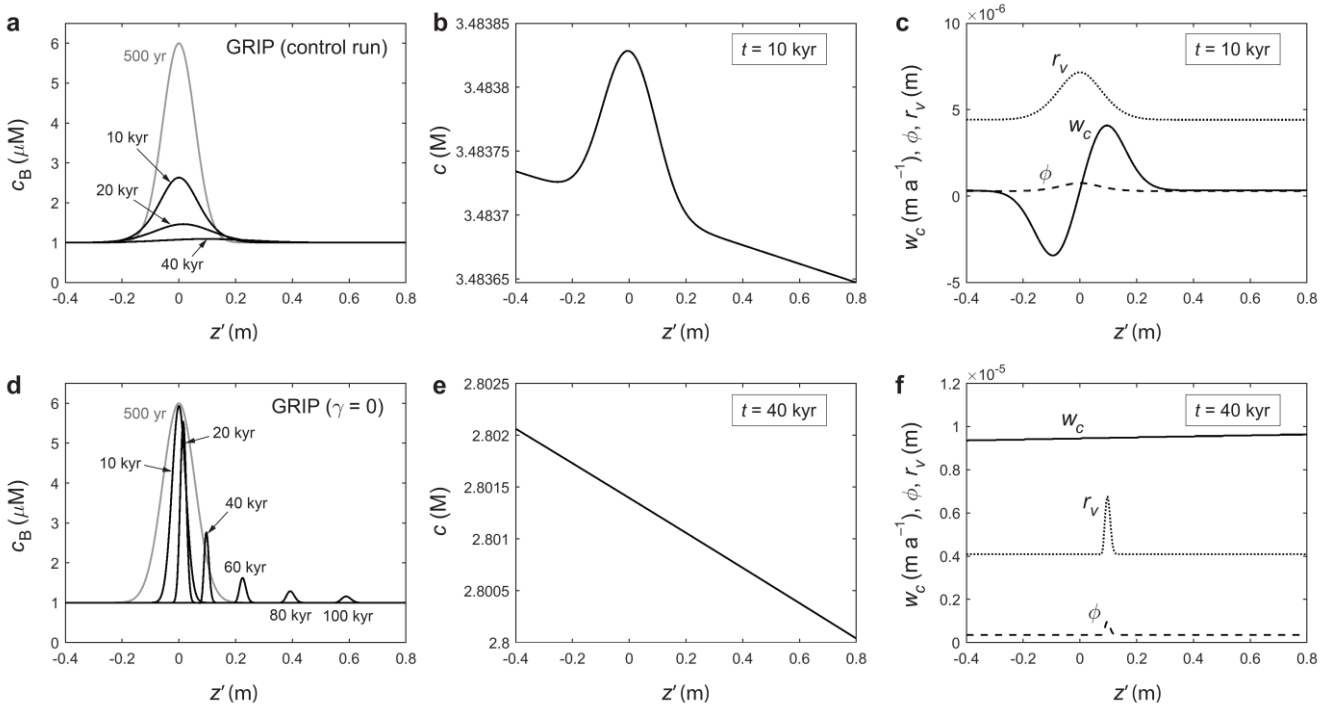


**Figure 4:** Modelled evolution of a signal peak in (a–c) the GRIP control run and (d–f) an otherwise identical run where the Gibbs–Thomson effect is turned off ($\gamma = 0$). Snapshots are shown in the material reference frame, with displacement $z'$ measuring how far the signal has moved from ice of the same age (which lies at $z' = 0$). (a,d) bulk solute concentration $c_B$; (b,e) vein solute concentration $c$ at one time; (c,f) anomalous velocity $w_c$, ice porosity $\phi$, vein curvature $r_v$ at one time. Grey curves in (a, d) indicate the initial doped peak. Panel b illustrates the Gibbs–Thomson perturbation. See Movie S1 for the full simulations.

785

https://doi.org/10.5194/tc-2020-217
Preprint. Discussion started: 7 September 2020


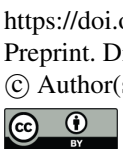



790

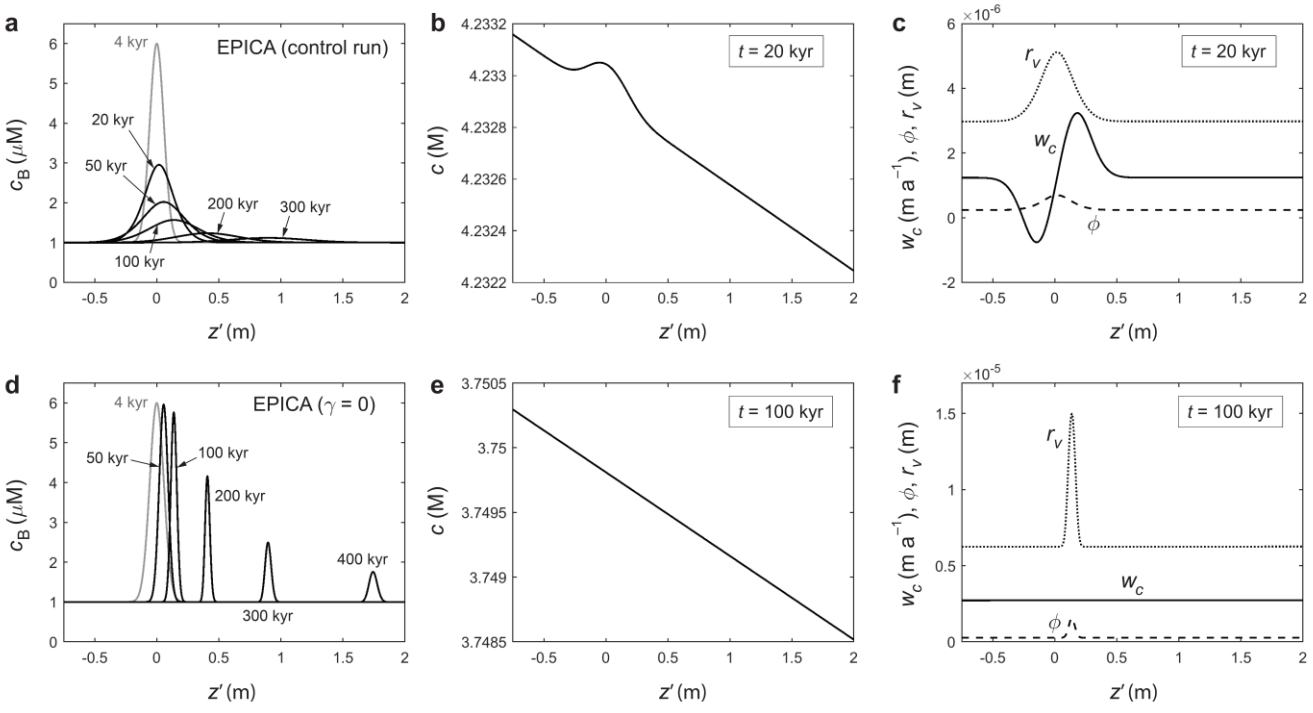


795

**Figure 5:** Modelled evolution of a signal peak in (a–c) the EPICA control run and (d–f) an otherwise identical run where the Gibbs–Thomson effect is turned off ($\gamma = 0$). (a,d) bulk solute concentration $c_B$; (b,e) vein solute concentration $c$ at one time; (c,f) anomalous velocity $w_c$, ice porosity $\phi$, vein curvature $r_v$ at one time. Grey curves in (a, d) indicate the initial doped peak. Panel b illustrates the Gibbs–Thomson

800 perturbation. See Movie S2 for the full simulations.

805

https://doi.org/10.5194/tc-2020-217
Preprint. Discussion started: 7 September 2020


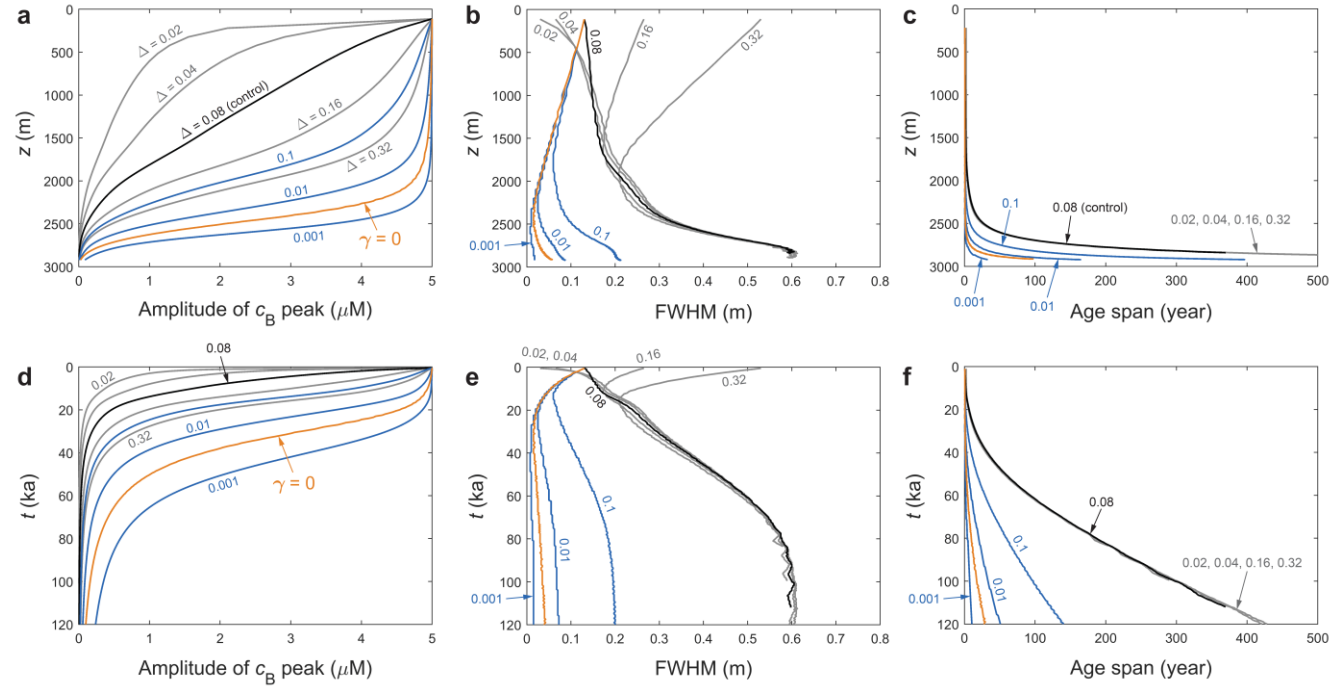


**Figure 6:** Changing morphometry of the signal peak – its amplitude, full width at half maximum (FWHM), age span – in the GRIP ice core for different model parameters, plotted against depth (a–c) and age of the ice (d–f). Black curves plot the control run of Fig. 4a, and orange curves the $\gamma = 0$ run of Fig. 4d. Grey curves plot the results of altering the width parameter $\Delta$ of the doped peak from 0.08 (control) to four other values. Blue curves plot the outcomes of suppressing molecular diffusivity $D$ in the control run by the multiplicative factors 0.1, 0.01 and 0.001, to simulate vein blockage. Parameter labels use the same colours as the curves. Peak width becomes difficult to measure as amplitude diminishes, explaining the jittery appearance of some curves at depth.

https://doi.org/10.5194/tc-2020-217
Preprint. Discussion started: 7 September 2020


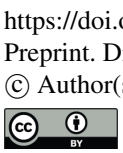

The Cryosphere Discussions
Open Access
EGU

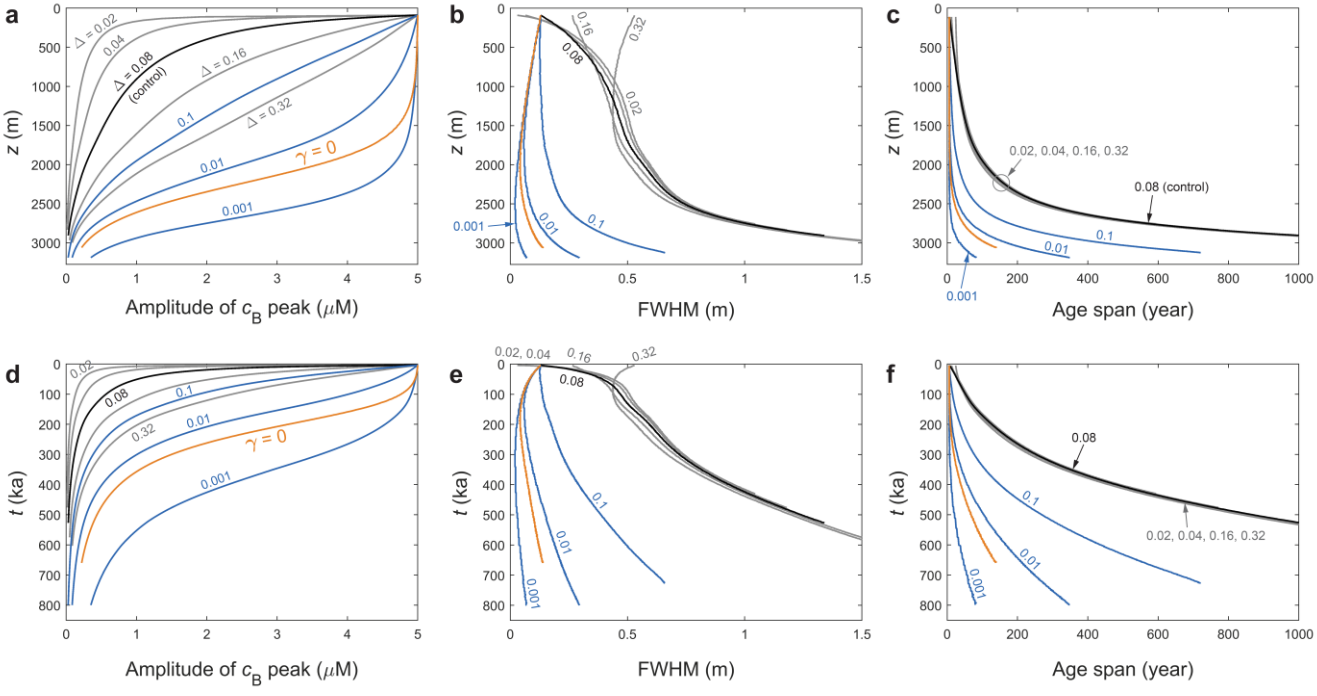


**Figure 7:** Changing morphometry of the signal peak – its amplitude, full width at half maximum (FWHM), age span – in the EPICA ice core for different model parameters, plotted against depth (a–c) and age of the ice (d–f). Black curves plot the control run of Fig. 5a, and orange curves the $\gamma = 0$ run of Fig. 5d. Grey and blue curves document the same sensitivity tests as conducted for the GRIP core (see caption of Fig. 6 for details).

https://doi.org/10.5194/tc-2020-217
Preprint. Discussion started: 7 September 2020


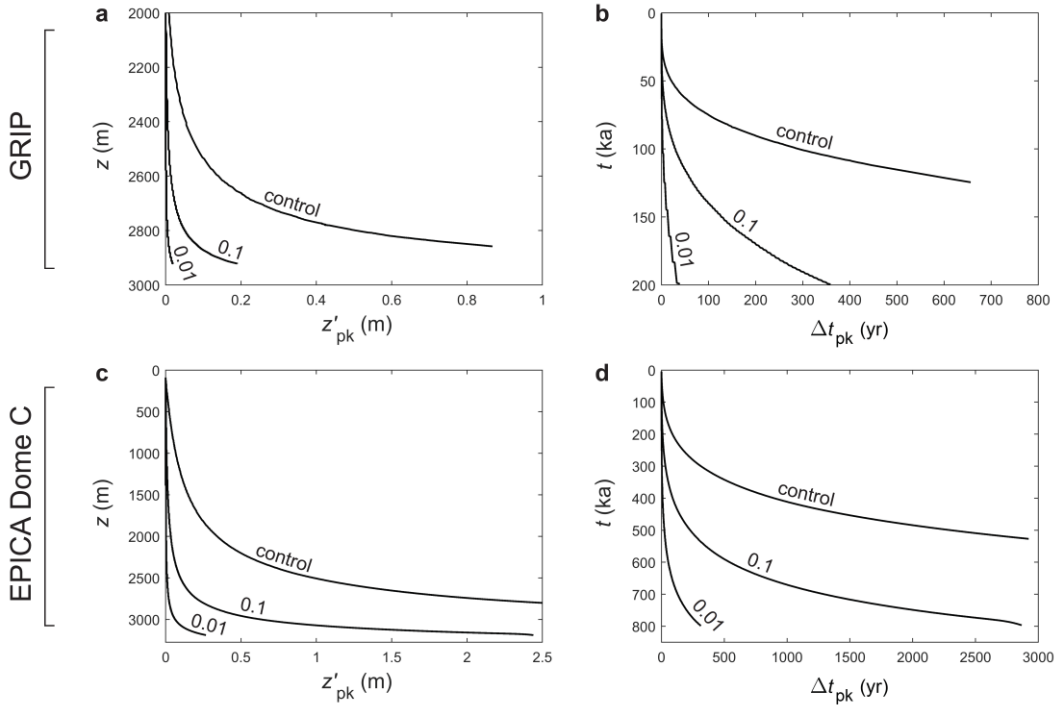


**Figure 8:** Modelled displacement $z'_{pk}$ and age offset $\Delta t_{pk}$ of signal peaks (from ice of the same age) at the (a,b) GRIP and (c,d) EPICA core sites for different parameters, plotted against depth and age of the ice. "Control" labels the control runs in Figs. 4a and 5a; 0.1 and 0.01 label those runs in Figs. 6 and 7 where the molecular diffusivity $D$ is suppressed by these factors to simulate vein blockage. The control curve in panel a is equivalent to the curve in Fig. 4 of Rempel et al. (2001), except they assumed a different age-depth scale from ours.

https://doi.org/10.5194/tc-2020-217
Preprint. Discussion started: 7 September 2020




870

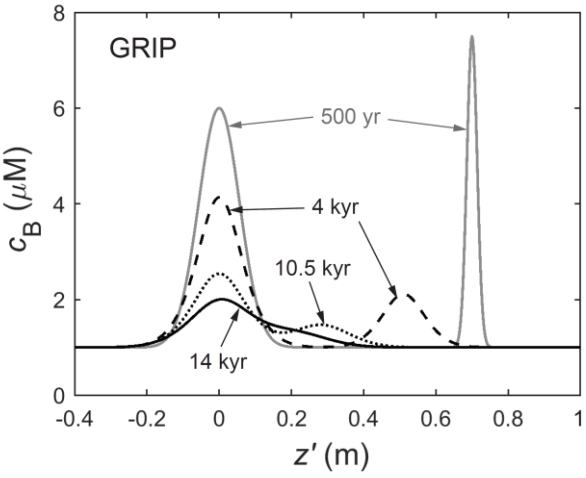


875 **Figure 9:** Snapshots (at four times) from the evolution of two neighbouring peaks in a GRIP run that uses the control parameters of the run in Fig. 4a. Diffusional spreading causes the peaks to merge as they approach each other under vertical compression. See Movie S3 for the full simulation.

880

885

890

https://doi.org/10.5194/tc-2020-217
Preprint. Discussion started: 7 September 2020


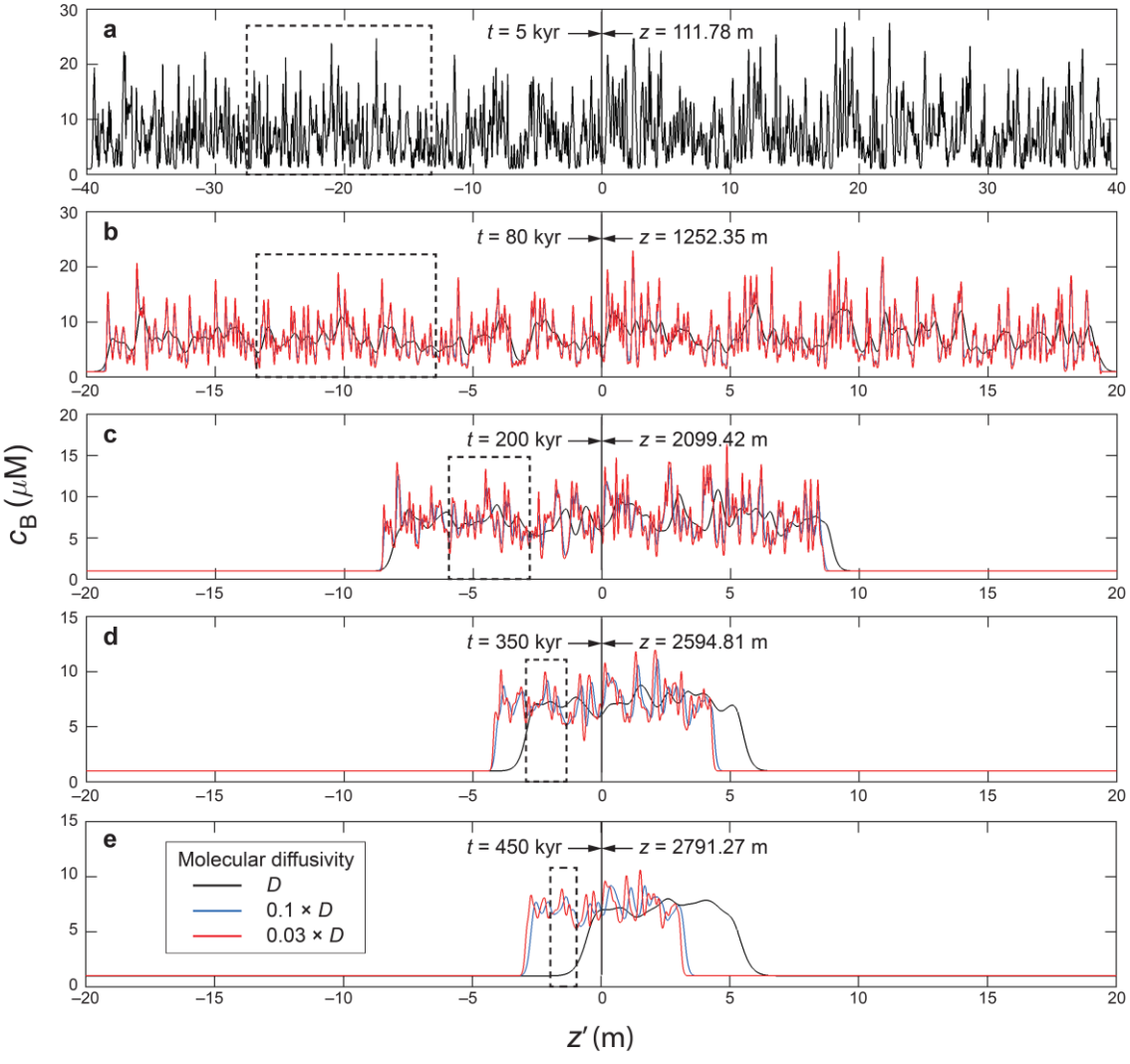


**Figure 10:** Simulated evolution of a long sequence of doped signals at the EPICA site, in three experiments assuming the molecular diffusivities $D$ (Table 1), $0.1D$ and $0.03D$. (a) Initial $c_B$ sequence. Used in all three runs and made from the superposition of 1200 decimetre-scale Gaussian peaks, it is not meant to recreate the actual signals at EPICA. (b)–(e) Snapshots of $c_B$ at later times. Labels near the vertical line indicate the depth and age of the ice at $z' = 0$. The dashed boxes trace a group of signals as they evolve into new signals through compression-diffusion merging (Sect. 3.3). As $D$ is reduced, signal persistence into deep ice improves, and signal displacement decreases. The duration of the signal sequence is ≈ 3,600 yr in all panels. See Movie S5 for the full simulations.

https://doi.org/10.5194/tc-2020-217
Preprint. Discussion started: 7 September 2020


The Cryosphere Discussions
Open Access
EGU

905

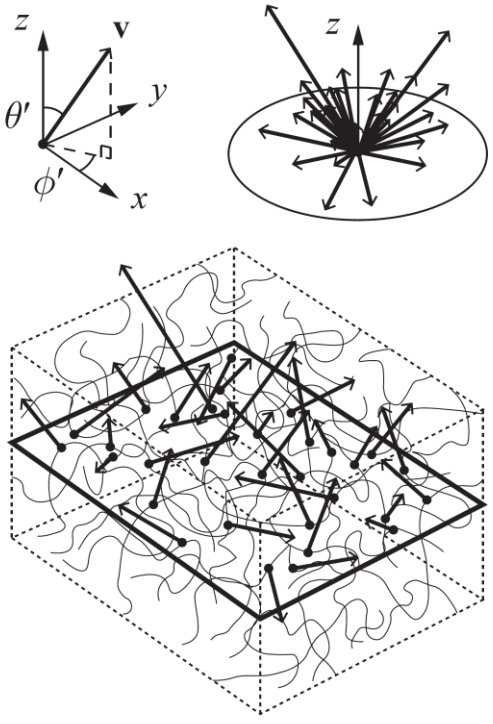


910 **Figure B1:** Velocities **v** of different vein segments crossing a plane (outlined by bold rectangle), and their distribution in spherical coordinates (upper right). Only crossings in one direction are shown. In Appendix B, a statistical theory is used to calculate the net transport of porosity and vein impurity resulting from this motion.

915

920

https://doi.org/10.5194/tc-2020-217
Preprint. Discussion started: 7 September 2020




925

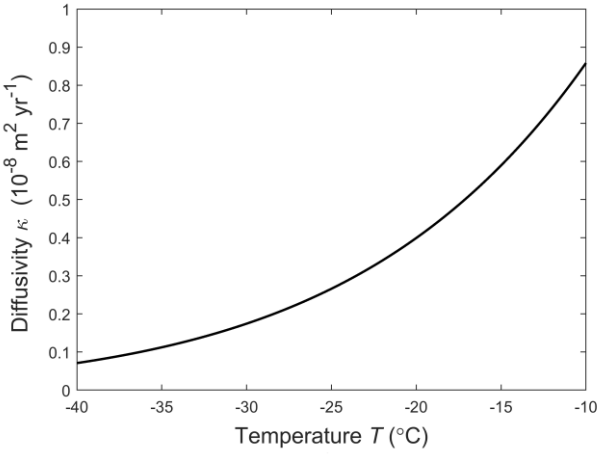


**Figure B2:** Diffusivity $\kappa$ at different temperatures, calculated with (9) for $c_1 = 2.5$.

930